

# Atezolizumab following definitive chemoradiotherapy in patients with unresectable locally advanced esophageal squamous cell carcinoma – a multicenter phase 2 trial (EPOC1802)

Received: 15 March 2024

Accepted: 21 January 2025

Published online: 19 February 2025

 Check for updates

A list of authors and their affiliations appears at the end of the paper

Platinum-based definitive chemoradiotherapy (dCRT) is the standard treatment for patients with unresectable locally advanced esophageal squamous cell carcinoma (ESCC) that invades the aorta, vertebral body or trachea; however, complete response rates remain low (11–25%), leading to poor survival. To evaluate the additive efficacy of the anti-PD-L1 antibody drug atezolizumab, we conducted a phase 2, multicenter, single-arm trial of 1 year of atezolizumab treatment following dCRT in 40 patients with unresectable locally advanced ESCC recruited from seven Japanese centers (UMIN000034373). The confirmed complete response (cCR) rate (primary end point) of the first consecutive 38 patients was 42.1% (90% CI 28.5–56.7%). Regarding the secondary end points, the median progression-free survival and 12-month progression-free survival rates of all 40 patients were 3.2 months and 29.6%, respectively, and the preliminary median overall survival with short-term follow-up and 12-month overall survival rate were 31.0 months and 65.8%, respectively. Other secondary end points evaluated included the cCR rate determined by an investigator's assessment in the locoregionally recurrent ESCC cohort, cCR rate determined by central assessment, overall response rate and incidence of adverse events. No treatment-related death occurred during the study. Atezolizumab monotherapy after dCRT resulted in a promising cCR rate, although long-term survival data are required.

Esophageal cancer ranks as the seventh most prevalent cancer and the sixth leading cause of cancer-related deaths worldwide, accounting for more than half a million cancer-related mortality annually<sup>1</sup>. According to the Comprehensive Registry of Esophageal Cancer in Japan, ESCC invading adjacent structures, such as the aorta, vertebral bodies or trachea (T4b), accounts for approximately 6.7% of all cases of esophageal cancer (approximately 1,500 patients per year in Japan)<sup>2</sup>. As T4b ESCC is unresectable, the standard treatment globally is dCRT with curative

intent using platinum-based regimen plus 50–60 Gy of radiation<sup>3–5</sup>; however, clinical trial results using this regimen have shown that cCR rates are low (11–25%), resulting in a median overall survival (OS) of 9–10 months<sup>6–8</sup>. Recent real-world data from 175 patients with unresectable locally advanced ESCC from 2013 to 2020 indicated that the cCR rate was 24% (ref. 9), as treatment regimens have not changed since the 1990s (ref. 10). Therefore, new treatment regimens with improved response and survival rates are urgently required.

✉ e-mail: [hbando@east.ncc.go.jp](mailto:hbando@east.ncc.go.jp); [takojima@east.ncc.go.jp](mailto:takojima@east.ncc.go.jp)

Among such treatment regimens, immunotherapy with immune-checkpoint inhibitors (ICIs) including anti-cytotoxic T-lymphocyte-associated protein 4 (CTLA-4), anti-PD-1 and anti-PD-L1 antibodies has revolutionized the treatment of advanced cancers, including esophageal cancer. Currently, 5-FU/cisplatin + pembrolizumab, 5-FU/cisplatin + nivolumab, and nivolumab + ipilimumab are the standard first-line therapies for patients with advanced metastatic ESCC<sup>3,11,12</sup>. In addition, in patients with resectable locally advanced esophageal adenocarcinoma and ESCC, neoadjuvant CRT followed by surgery and adjuvant 1-year nivolumab has been the standard therapy<sup>3,13,14</sup>; however, the efficacy and safety of ICIs in patients with unresectable locally advanced ESCC treated with dCRT remain unclear.

Basic research suggests that the use of ICIs combined with ionizing radiation is a promising approach, owing to the synergistic efficacy of these therapies. The mechanisms by which radiation facilitates ICI activity include increased tumor antigen release, activated innate immune system, increased T cell infiltration, increased antigen presentation and modulated immunosuppressive cells<sup>15,16</sup>. Chemotherapy and radiotherapy may mediate the release of interferon (IFN)- $\gamma$  produced by CD8<sup>+</sup> T cells, resulting in PD-L1 upregulation in various tumor cells<sup>16,17</sup>. As lymphocytes are radiation sensitive, we hypothesized that sequential combinations of anti-PD-L1 agents immediately after CRT completion would enhance the therapeutic efficacy of the anti-PD-L1 agent. Indeed, among patients with unresectable locally advanced cell lung cancer, 12 months of treatment with the anti-PD-L1 antibody durvalumab after platinum-based CRT significantly improved both progression-free survival (PFS) and OS, irrespective of PD-L1 expression before CRT<sup>18,19</sup>.

Based on this information, we planned a phase II proof-of-concept clinical trial (EPOC1802, TENERGY) to evaluate the safety and efficacy of the anti-PD-L1 antibody atezolizumab following definitive CRT in patients with unresectable, locally advanced ESCC.

## Results

### Patient characteristics and treatment protocol

In this phase II study, patients with unresectable locally advanced ESCC treated with two cycles of cisplatin/5-FU plus 60 Gy of radiation were enrolled. The treatment consisted of atezolizumab monotherapy every 3 weeks for a maximum of 12 months (Fig. 1a). Of the 51 candidate patients with unresectable locally advanced ESCC who were treated with dCRT, 2 patients with lung metastasis after CRT, 3 patients with prolonged CRT-related adverse events, 2 patients who refused to participate, 1 patient with tracheal fistula after CRT, 1 patient whose general condition deteriorated and 2 patients treated with ineligible radiation were not included in the study. Thus, 40 patients were enrolled in the primary cohort between December 2018 and March 2021. In addition, ten patients with locoregionally recurrent ESCC after radical surgery were enrolled in the exploratory cohort because additional surgical resection is difficult and they are generally treated with dCRT. Sex was not considered in the study design and the sex of the participants was determined based on self-reports. In the primary cohort, the median age was 64 years and 82.5% (33 of 40) of the patients were male (Table 1). A total of 95.0% (38 of 40) of patients had clinical T4 disease and 92.5% (37 of 40) had lymph node metastasis. Furthermore, 25.0% (10 of 40) of the patients had extraregional M1 lymph node metastasis. Accordingly, 97.5% of the patients were diagnosed with clinical stage IVA or IVB ESCC (Table 1).

In the primary cohort, the median relative dose intensity (RDI) for atezolizumab was 97.3%. Most patients discontinued atezolizumab due to disease progression (57.5%, 23 of 40), and 27.5% (11 of 40) completed atezolizumab monotherapy (Supplementary Table 1). The median RDI of atezolizumab was 95.6% and 60.0% (6 of 10) of the patients in the exploratory cohort discontinued owing to disease progression.

### Efficacy and adverse events

Because long-term survival with dCRT is expected only in patients with cCR, we decided that the cCR rate determined by an investigator's

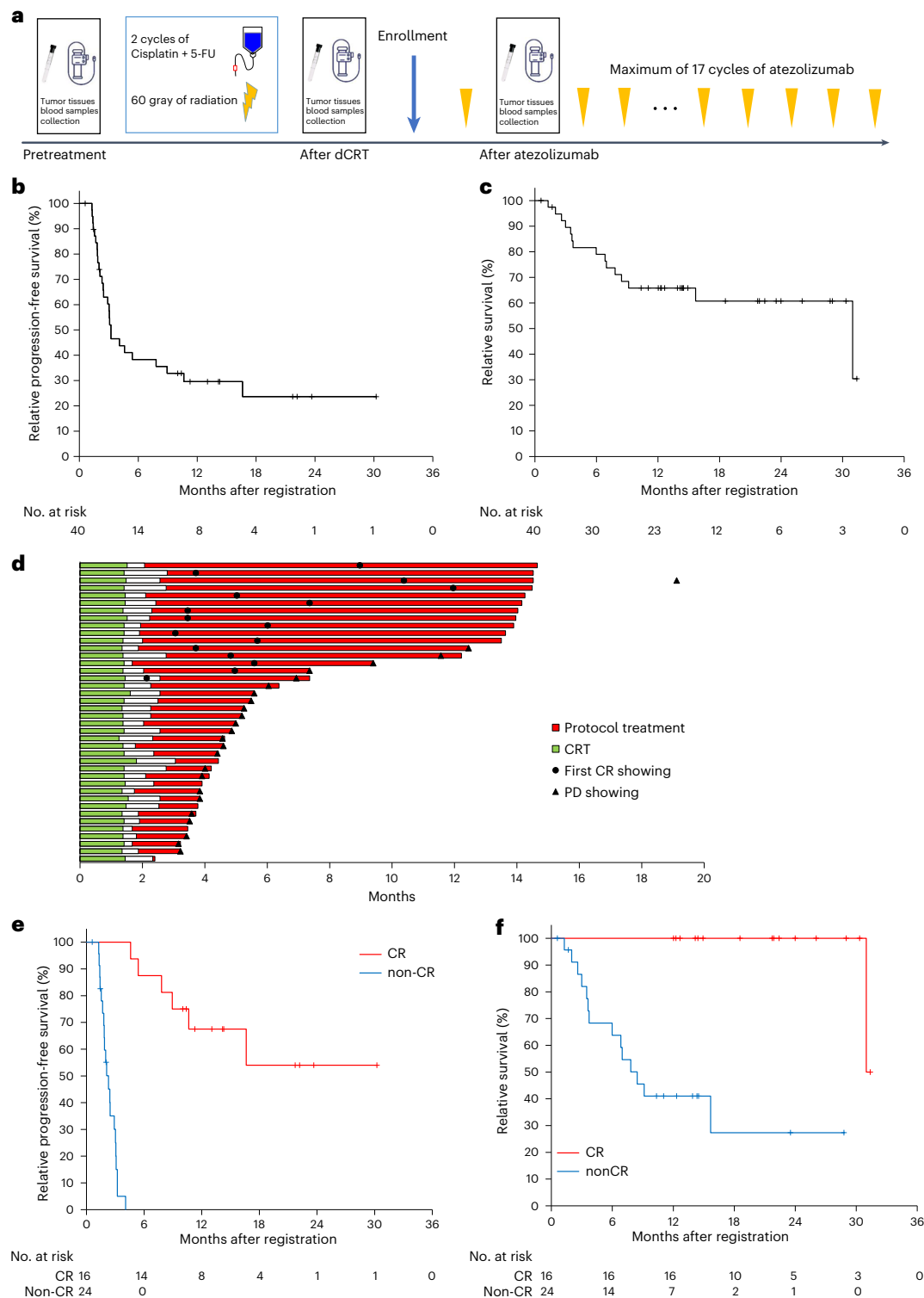
assessment in the primary cohort was the primary end point in this study. The cCR rate of the first consecutive 38 patients in the primary cohort was 42.1% (90% confidence interval (CI) 28.5–56.7%). As the lower limit of the 90% CI for the cCR rate was >20%, the primary end point was met. Thus, this treatment merits further development. The cCR rates in the primary and exploratory cohorts were 40.0% and 50.0%, respectively (Table 2). In addition, of the 51 candidate patients treated with dCRT in the primary cohort, the cCR rate was 35.3% (18 of 51), as 2 of the 11 (18.2%) patients who were not included in the trial exhibited cCR. In the primary cohort, the median follow-up period was 12.5 (range 0.6–31.4) months. The median PFS and 12-month PFS rate were 3.2 months and 29.6%, respectively (Fig. 1b). Of the 25 patients with disease progression, 16 had local regrowth, 6 had metastatic disease, 2 had both and 1 had clinical disease progression. After the study treatment, radical resection and additional dCRT were performed in seven (one before and six after PFS events) and two patients, respectively. Palliative radiotherapy, another ICI and chemotherapy were administered to 5, 3 and 19 patients, respectively (Supplementary Table 2). At a median follow-up duration of 12.5 (range 0.6–31.4) months, the median OS and 12-month OS rate were 31.0 months and 65.8%, respectively (Fig. 1c,d). We determined the median PFS and OS from the starting date of dCRT, which is the common starting date, at 5.5 and 33.0 months, respectively. In patients with cCR, the median PFS was not reached, and the 12-month PFS rate was 67.5%; only one patient died (Fig. 1e,f). Of the 35 patients with evaluable PD-L1 tumor proportion score (TPS), the cCR rates with PD-L1 TPS < 1% and  $\geq$ 1% were not significantly different at 44.4% and 41.2%, respectively (Supplementary Table 3). The peripheral blood lymphocyte counts decreased during dCRT and recovered during the study period. The lowest peripheral blood lymphocyte counts were not significantly different between patients with and without cCR (Supplementary Table 4).

Although 5.0% and 10.0% of patients in the primary and exploratory cohorts, respectively, showed grade 3 or higher pneumonitis, only one (2.5%) case of grade 2 adrenal insufficiency, one (2.5%) with grade 1 hyperthyroidism and three (7.5%) with grades 1–2 hypothyroidism were observed in the primary cohort. No treatment-related deaths were observed (Supplementary Table 5). Atezolizumab monotherapy following dCRT increases long-term survival without compromising safety.

### Combined dCRT/atezolizumab strengthens antitumor response

To investigate the predictive biomarkers, we performed serial biopsies of the primary tumor and collected blood samples at three time points (before treatment, after dCRT and 4 weeks after the first atezolizumab dose) (Fig. 1a). We used these samples to assess whether dCRT could strengthen antitumor immune responses in the tumor microenvironment (TME). First, we compared the immune-related gene expression in ESCC biopsy samples before and after dCRT. Gene set expression analysis (GSEA) using Gene Ontology Biological Process (GOBP) gene sets showed that both gene signatures related to innate and acquired immunity were significantly upregulated by dCRT (Fig. 2a). Furthermore, consistent with previous reports<sup>20–23</sup>, the GSEA results suggest that tumor cells released cytoplasmic DNA and RNA when exposed to dCRT and activated cytosolic DNA- and RNA-sensing pathways (the cGAS–STING pathway<sup>20,21</sup> and RIG-I pathway<sup>22,23</sup>, respectively) (Extended Data Fig. 1a). Furthermore, tumors exhibited type I and II IFN responses<sup>16,17,20–23</sup> (Extended Data Fig. 1b) and *HLA-A*, *HLA-B* and *HLA-C* upregulation<sup>24</sup> ( $n = 28$ ) (Extended Data Fig. 1c). These phenomena promoted TCR stimulation, co-stimulation by CD28 and further PD-1 signaling<sup>15–17</sup> (Extended Data Fig. 1d). Consistent with these findings, we found that, among the immune-checkpoint molecules, the expression of *CD274* was significantly increased by dCRT ( $n = 28$ ) (Extended Data Fig. 1e).

In addition, we calculated single-sample GSEA (ssGSEA) scores<sup>25</sup> during the treatment course ( $n = 28$ ) (Fig. 2b and Extended Data



**Fig. 1 | Study design and patient survival. a**, In this phase II study, patients with unresectable locally advanced ESCC treated with two cycles of cisplatin/5-FU plus 60 Gy of radiation were enrolled. The study treatment was 12 months of atezolizumab monotherapy every 3 weeks. For the biomarker study, serial biopsies from the primary site and blood collection were performed at three time points (before treatment, after definitive chemoradiotherapy and 4 weeks after the first atezolizumab dose). **b, c**, Kaplan–Meier plots of PFS ( $n = 40$  patients) and OS ( $n = 40$  patients) in the primary cohort for primary unresectable locally

advanced ESCC are shown. Vertical lines denote patients who were censored. **d**, Swimmer plots of dCRT, the treatment protocol, first CR and PD in the primary cohort ( $n = 40$  patients) are shown. **e, f**, Kaplan–Meier plots of PFS (cCR group,  $n = 16$  patients, non-cCR group,  $n = 24$  patients) and OS (cCR group,  $n = 16$  patients; non-cCR group,  $n = 24$  patients) in patients with cCR (red) and without cCR (blue) in the primary cohort are shown. Vertical lines denote patients who were censored.

**Table 1 | Patient characteristics**

	Primary cohort (n=40)	Exploratory cohort (n=10)
Age, median (range)	64 years (45–79)	64 years (51–72)
Sex, male/female (%)	33 (82.5)/7 (17.5)	8 (80.0)/2 (20.0)
ECOG PS, 0/1 (%)	32 (80.0)/8 (20.0)	9 (90.0)/1 (10.0)
Location of primary lesion, upper/middle/lower (%)	11 (27.5)/26 (65.0)/ 3 (7.5)	3 (30.0)/6 (60.0)/ 1 (10.0)
Length of primary lesion, median (range)	6 cm (2.6–15)	6 cm (2.0–25.0)
≤T3/T4 (%)	2 (5.0)/38 (95.0)	10 (100.0)/0 (0.0)
N0/N1/N2/N3 (%)	3 (7.5)/16 (40.0)/ 10 (25.0)/11 (27.5)	3 (30.0)/3 (30.0)/ 2 (20.0)/2 (20.0)
M0/M1 (%)	30 (75.0)/10 (25.0)	9 (90.0)/1 (10.0)
Stage ≤II/III/IVA/IVB (%)	0 (0.0)/1 (2.5)/ 29 (72.5)/10 (25.0)	5 (50.0)/3 (30.0)/ 1 (10.0)/1 (10.0)

1:ECOG PS, Eastern Cooperative Oncology Group Performance Status.

Fig. 1f). The combination of dCRT and sequential atezolizumab robustly increased the ssGSEA scores, reflecting the expression of the gene sets, General\_lymphocyte, Lineage\_cytotoxicT, IFNG\_28-gene, Lineage\_CD4, Lineage\_CD8, Lineage\_B\_cell and Lineage\_NK\_cell, but significantly decreased the ssGSEA scores, reflecting the expression of the gene sets Cell\_cycle\_G1S, Cell\_cycle\_G2M and MDSC\_ShirleyLiu. These data suggest that dCRT not only directly kills tumor cells, but also enhances antitumor immune responses, possibly increasing the efficacy of sequential atezolizumab treatment.

Next, we performed flow cytometry (FCM) to assess the immunological phenotypes of tumor-infiltrating lymphocytes (TILs) during the course of treatment ( $n = 18$ ) (Fig. 2c–e and Extended Data Fig. 2a). The ratio of CCR7<sup>+</sup>CD45RA<sup>+</sup> (effector memory (EM)) CD8<sup>+</sup>CD3<sup>+</sup> T cells to effector regulatory T (eT<sub>reg</sub>) cells, defined as FOXP3<sup>high</sup>CD45RA<sup>+</sup>CD4<sup>+</sup>CD3<sup>+</sup> T cells<sup>26</sup> and the proportions of Ki-67<sup>+</sup> and/or EOMES<sup>+</sup>T-bet<sup>+</sup> cells, which were regarded as effector T cells<sup>27</sup> in CD8<sup>+</sup> T cells were significantly elevated by dCRT, whereas PD-1 expression in CD8<sup>+</sup> T cells was slightly but not significantly elevated ( $n = 18$ ) (Fig. 2c and Extended Data Fig. 2a). The proportion of eT<sub>reg</sub> cells among the CD45<sup>+</sup> cells decreased during treatment (Extended Data Fig. 2b). Consistent with these results, multiplexed immunohistochemistry (mIHC) revealed a mild, although nonsignificant, increase in intratumor CD8<sup>+</sup>CD3<sup>+</sup> T cells and PD-1<sup>+</sup>CD8<sup>+</sup>CD3<sup>+</sup> T cells, likely because of the small sample size, and that intratumor FOXP3<sup>+</sup>CD8<sup>+</sup>CD3<sup>+</sup> T cells, which are indicative of T<sub>reg</sub> cells, were decreased ( $n = 40$ ) (Extended Data Fig. 2c,d). Furthermore, CTLA-4 expression on the surface of eT<sub>reg</sub> cells was increased by dCRT, although PD-1 expression in eT<sub>reg</sub> cells did not increase ( $n = 18$ ) (Extended Data Fig. 2b). dCRT increased not only the frequency of antigen-presenting cells (APCs), defined as HLA-DR<sup>+</sup>CD11c<sup>+</sup>CD45<sup>+</sup> cells, among CD45<sup>+</sup> cells, but also the expression of CD80, CD86 and PD-L1 in APCs ( $n = 18$ ) (Figs. 2d,e and Extended Data Fig. 2e). APC-induced PD-L1 expression increased after CRT and decreased after atezolizumab treatment. This result should be interpreted with caution because atezolizumab occupies the binding site of the anti-PD-L1 antibody used for FCM analysis (Extended Data Fig. 2f). Nonetheless, the FCM and mIHC data support the notion that dCRT recruits and activates APCs and effector T cells in the TME.

We performed FCM to evaluate the phenotypes of peripheral blood mononuclear cells (PBMCs) during the treatment course involving the combination of dCRT and sequential atezolizumab. This treatment combination increased the proportion of CD8<sup>+</sup>CD3<sup>+</sup> T cells among CD45<sup>+</sup> cells and Ki-67 expression in CD8<sup>+</sup> T cells ( $n = 17$ ) (Extended Data Fig. 3a). The proportion of eT<sub>reg</sub> cells among CD45<sup>+</sup> cells, expression of CTLA-4 and PD-1 on eT<sub>reg</sub> cells, ratio of CCR7<sup>+</sup>CD45RA<sup>+</sup> (EM) CD8<sup>+</sup>CD3<sup>+</sup>

**Table 2 | Confirmed complete response and overall response rates**

	Primary analysis (n=38) <sup>b</sup>	Primary cohort (n=40)	Exploratory cohort (n=10)
cCR rate (95% CI)	42.1% (28.5–56.7) <sup>c</sup>	40.0% (24.9–56.7)	50.0% (18.7–81.3)
Overall response rate <sup>a</sup> (95% CI)	65.8% (48.6–80.4)	62.5% (45.8–77.3)	80.0% (44.4–97.5)

<sup>a</sup>The overall response rate was evaluated based on the Response Evaluation Criteria in Solid Tumors v1.1. <sup>b</sup>We calculated the sample size of the primary locally advanced ESCC cohort at 38 with a CR of 40% deemed promising and one of 20% deemed unacceptable (one-sided  $\alpha$ , 0.05;  $\beta$ , 0.2). <sup>c</sup>90% CI.

T cells to eT<sub>reg</sub> cells, and expression of CD80, CD86 and PD-L1 on APCs were not significantly altered during treatment ( $n = 17$ ) (Extended Data Fig. 3b,c). These PBMC data suggest that combining dCRT and sequential atezolizumab treatment could strengthen the systemic antitumor immune response, especially that caused by effector CD8<sup>+</sup> T cells, in addition to the antitumor immune response in the TME.

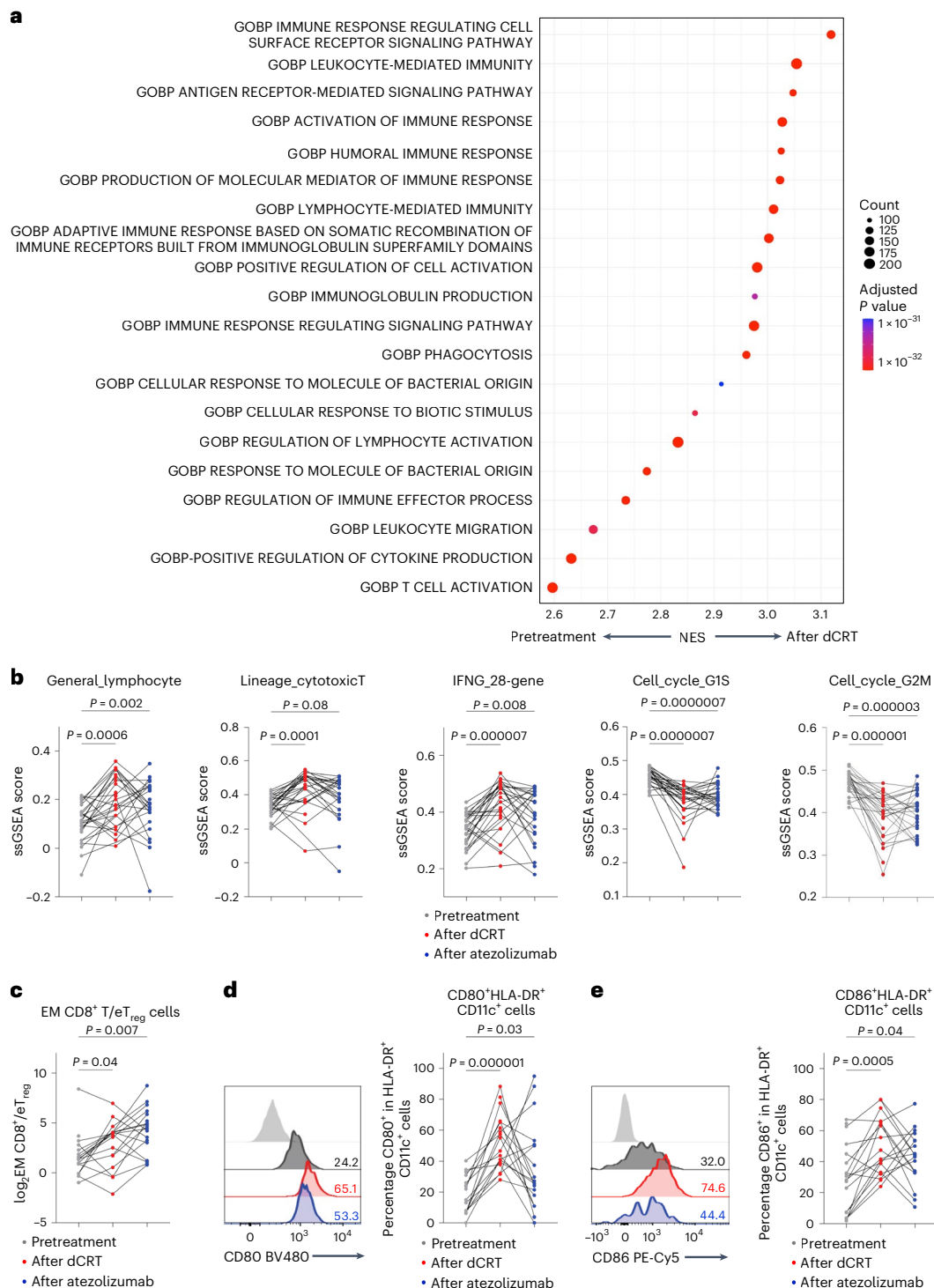
Collectively, these data from genomic and immunological analyses suggest that dCRT enhances IFN responses in tumor cells via cytoplasmic DNA- and RNA-sensing pathways and recruits and activates APCs and effector T cells in the TME. Consequently, augmented PD-L1 expression in APCs strengthens PD-1 signaling in effector T cells and hampers efficient antitumor immune responses. These findings support our hypothesis that sequential administration of anti-PD-L1 agents immediately after completing dCRT could vigorously enhance antitumor immune responses and optimize clinical efficacy.

### Genomic and immunological ESCCs analysis before treatment

To identify possible predictive biomarkers, we analyzed the genomic status of 27 ESCCs in the primary cohort before treatment. Whole-exome sequencing (WES) showed *MYC* amplification ( $n = 2$ ), *EGFR* mutation ( $n = 1$ ), *PIK3CA* mutation ( $n = 1$ ), *PTEN* mutation ( $n = 1$ ) and *KEAP1* mutation ( $n = 1$ ), which have been reported to be associated with ICI resistance mechanisms<sup>28–33</sup>, in 17 patients with non-cCR ( $n = 27$ ) (Fig. 3a). Tumor mutational burden (TMB) was not significantly associated with patient outcomes ( $n = 27$ ) (Fig. 3b). GSEA of HALLMARK gene sets demonstrated that gene expression signatures reflective of epithelial–mesenchymal transition (EMT) and TGF- $\beta$  signaling were significantly enriched in patients with non-cCR before dCRT (Fig. 3c), which is consistent with previous reports suggesting that cancers with these phenotypes can be resistant to cancer immunotherapy<sup>34,35</sup>. Furthermore, differentially expressed genes (DEGs) in ESCCs in the primary cohort were significantly associated with patient outcomes (Fig. 3d). Although neither the gene expression of human leukocyte antigen (HLA) and immune-checkpoint molecules nor the ssGSEA scores for immune-related gene sets before treatment were significantly associated with patient outcomes ( $n = 28$ ) (Extended Data Fig. 4a–c), *MMP1* and *MMP13* were significantly expressed in non-cCR patient tumors (Fig. 3d,e). Matrix metalloproteinase (MMP) family members, including *MMP1* and *MMP13*, are reportedly associated with EMT<sup>36,37</sup>, which probably causes resistance to various treatment strategies, including radiotherapy<sup>38</sup> and immunotherapy<sup>35</sup>.

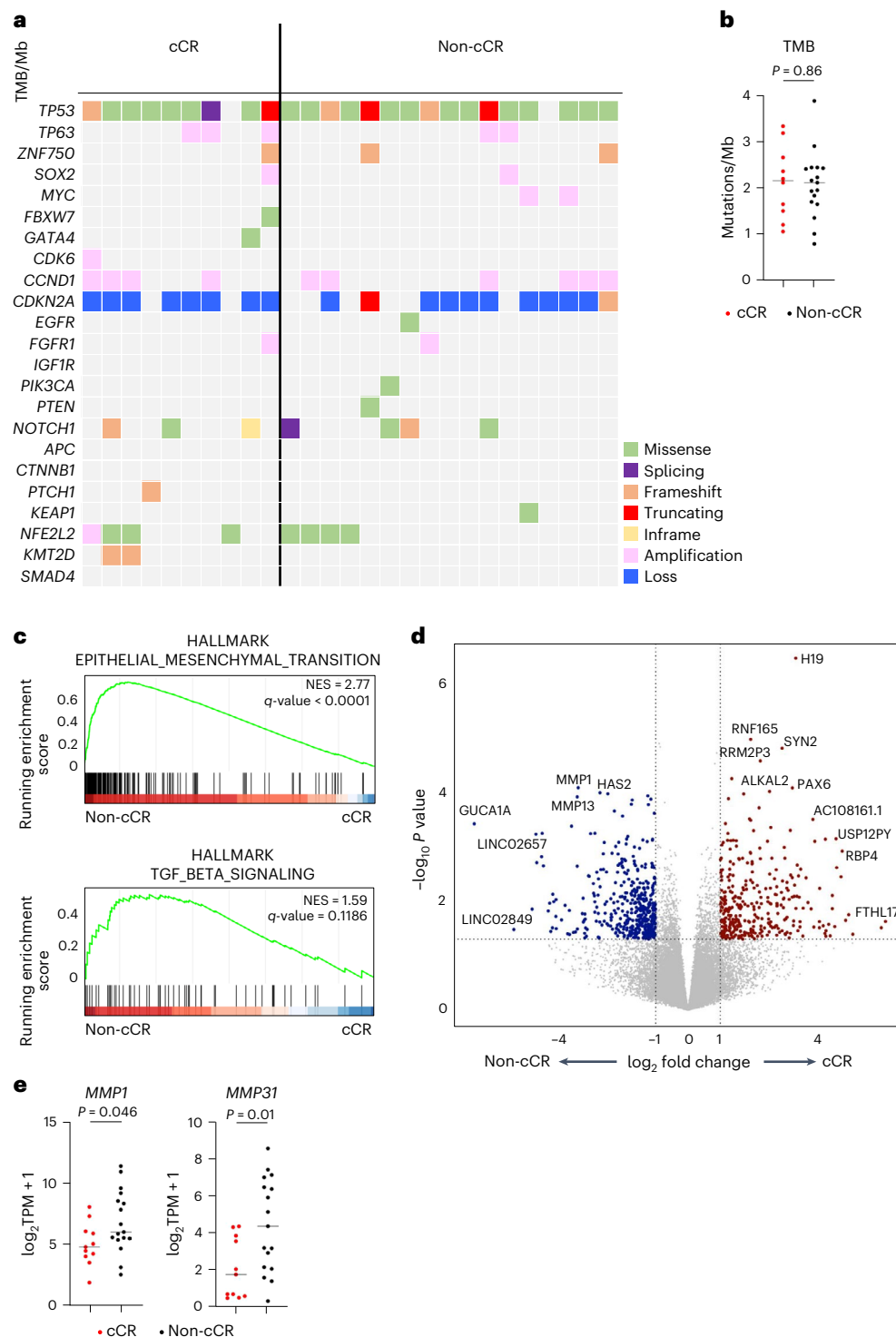
Next, we evaluated the immunological phenotypes of TILs by FCM and mIHC (Fig. 4a–d and Extended Data Fig. 5a–c). According to FCM analysis, PD-1 expression in CD8<sup>+</sup> T cells was significantly higher in patients who achieved cCR than in those who did not ( $n = 18$ ) (Fig. 4a), whereas other parameters before treatment were not significantly associated with patient outcomes ( $n = 18$ ) (Fig. 4b–d and Extended Data Fig. 5a,b). Additionally, we performed mIHC analysis of the specimens before treatment and found that intratumor CD8<sup>+</sup>CD3<sup>+</sup> T cells and PD-1<sup>+</sup>CD8<sup>+</sup>CD3<sup>+</sup> T cells were significantly more abundant in patients





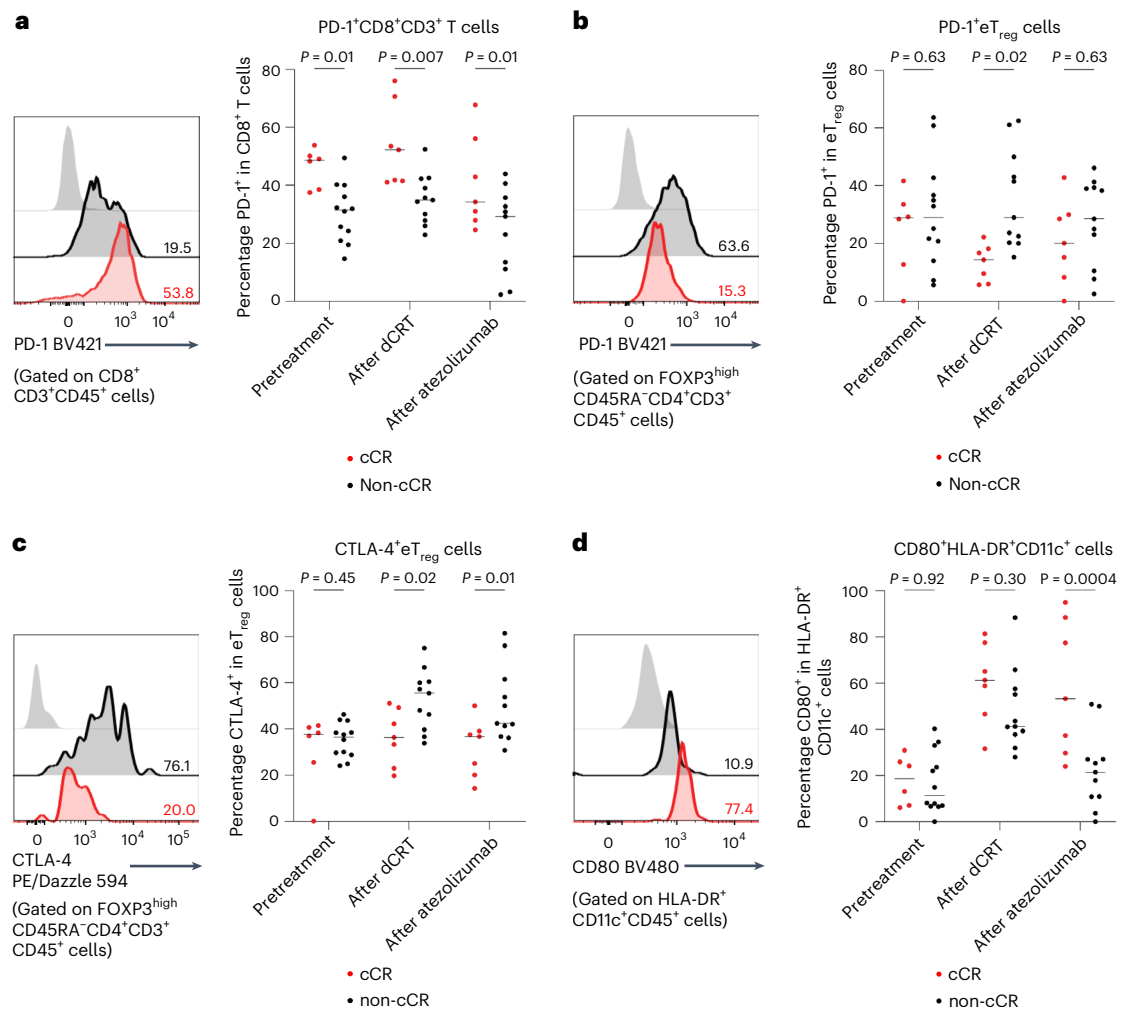
**Fig. 2 | Combination therapy with dCRT and atezolizumab strengthens antitumor immune responses. a,b**, RNA extracted from ESCCs during treatment (pretreatment ( $n = 28$  patients) after dCRT ( $n = 25$  patients) and after atezolizumab treatment ( $n = 25$  patients)) was subjected to RNA-seq. Gene expression in ESCCs after dCRT was compared to that in ESCCs before treatment by performing GSEA with GOBP gene sets (a). The top 20 significantly enriched gene sets among GOBP gene sets are shown. ssGSEA scores from the indicated gene sets were calculated from gene expression in ESCCs during treatment (b). Summaries of ssGSEA scores from the indicated gene sets are shown. Gray, pretreatment; red, after dCRT; blue, after atezolizumab (anti-PD-L1 mAb). c–e, TILs extracted from ESCCs during treatment (pretreatment ( $n = 18$  patients), after dCRT ( $n = 18$  patients) and after atezolizumab treatment ( $n = 18$  patients)) were subjected to FCM. Summary of the ratio of intratumor CCR7<sup>+</sup>CD45RA<sup>+</sup> (effector memory (EM)) CD8<sup>+</sup>CD3<sup>+</sup>CD45<sup>+</sup> T cells to FOXP3<sup>high</sup>CD45RA<sup>+</sup>CD4<sup>+</sup>CD3<sup>+</sup>CD45<sup>+</sup> T cells (eT<sub>reg</sub> cells) during treatment

(pretreatment, after dCRT and after atezolizumab treatment) is shown (c). Gray, pretreatment; red, after dCRT; blue, after atezolizumab (anti-PD-L1 mAb). Representative histograms (left) and summary (right) of CD80 (d) and CD86 (e) expression in HLA-DR<sup>+</sup>CD11c<sup>+</sup>CD45<sup>+</sup> cells (APCs) during treatment courses (pretreatment, after dCRT and after atezolizumab treatment) are shown. Gray, pretreatment; red, after dCRT; blue, after atezolizumab (anti-PD-L1 mAb); light gray, unstained control.  $P$  values were calculated by permutation testing in GSEA (a).  $P$  values were calculated by one-way analysis of variance (ANOVA) (b–e). For multiple comparisons, Holm–Sidak’s test was performed. The differences with  $P \leq 0.05$  were considered significant. Significant differences were found in general lymphocytes ( $P = 0.002$ ), lineage cytotoxic T ( $P = 0.08$ ), IFNG28 gene ( $P = 0.008$ ), cell cycle G1S ( $P = 0.0000007$ ), cell cycle G2M ( $P = 0.000003$ ), EM CD8<sup>+</sup> T/eT<sub>reg</sub> cells ( $P = 0.007$ ), CD80<sup>+</sup>HLA-DR<sup>+</sup>CD11c<sup>+</sup> ( $P = 0.03$ ) and CD86<sup>+</sup>HLA-DR<sup>+</sup>CD11c<sup>+</sup> ( $P = 0.04$ ) cells. mAb, monoclonal antibody.



**Fig. 3 | Comprehensive analysis of ESCCs before treatment. a,b,** DNA extracted from 27 pretreatment ESCC cases was subjected to WES. Representative driver gene alterations (filled sections) and the TMB (columns) are shown (a). Green, missense variants; purple, splicing variants; orange, frameshift; red, truncating mutations; yellow, in-frame mutations; pink, amplification; blue, loss. The TMB of ESCCs before treatment was compared between patients who achieved cCR ( $n = 10$ ) and those who did not ( $n = 17$ ) (b). **c,d,** RNA extracted from 27 pretreatment ESCCs was subjected to RNA-seq. Gene expression in non-cCR ESCC cases before treatment was compared to that in cCR ESCCs by performing GSEA with HALLMARK gene sets (c). Top and bottom show the results achieved by analyzing the expression of epithelial–mesenchymal transition-related genes and TGF- $\beta$  signaling-related genes, respectively. Volcano plots analyzing

enriched differential genes between non-cCR ESCC and cCR esophageal cancer samples (d). In brief, treatment are shown. Red shows patients who achieved cCR (cCR cases); blue shows patients who did not achieve cCR (non-cCR cases). **e,** Expressions of *MMP1* (left) and *MMP13* (right) in the ESCCs of cCR cases (red) and non-cCR cases (black) pretreatment (cCR,  $n = 11$  patients; non-cCR,  $n = 17$  patients) were evaluated. Summaries of the TPM values of *MMP1* (left) and *MMP13* (right) in the ESCCs of cCR cases (red) and non-cCR cases (black) are shown. Bars indicate mean.  $P$  values were calculated by unpaired two-tailed  $t$ -test, revealing significant differences in *MMP1* ( $P = 0.0458$ ) and *MMP13* ( $P = 0.0111$ ), but not TMB ( $P = 0.86$ ) between the cCR and non-cCR cases (b,e).  $P$  values were calculated using the likelihood ratio test (d). The differences with  $P \leq 0.05$  were considered significant. TPM, transcripts per million.



**Fig. 4 | Immunological analysis of TILs before, during and after combination therapy with dCRT and atezolizumab.** TILs extracted from ESCCs during treatment (pretreatment (cCR,  $n = 6$  patients; non-cCR,  $n = 12$  patients), after dCRT (cCR,  $n = 7$  patients; non-cCR,  $n = 11$  patients), and after atezolizumab treatment (cCR,  $n = 7$  patients; non-cCR,  $n = 11$  patients)) were subjected to FCM. **a–d**, Representative histograms (left) and summaries (right) of the frequencies of intratumor immune cells, including PD-1<sup>+</sup>CD8<sup>+</sup>CD3<sup>+</sup> T cells (**a**), PD-1<sup>+</sup>FOXP3<sup>high</sup>CD45RA<sup>+</sup>CD4<sup>+</sup>CD3<sup>+</sup> T cells (**b**), CTLA-4<sup>+</sup>FOXP3<sup>high</sup>CD45RA<sup>+</sup>CD4<sup>+</sup>CD3<sup>+</sup> T cells (**c**) and CD80<sup>+</sup>HLA-DR<sup>+</sup>CD11c<sup>+</sup>CD45<sup>+</sup> cells (**d**), during treatment (pretreatment, after dCRT and after atezolizumab treatment) are shown according to treatment response. Gray, unstained control; red, patients who achieved cCR (cCR cases);

black, patients who did not achieve cCR (non-cCR cases). Bars, mean;  $P$  values were calculated using two-way ANOVA. The Holm–Sidak test was performed for multiple comparisons. The differences with  $P \leq 0.05$  were considered significant. Significant differences between the cCR and non-cCR cases were found for PD-1<sup>+</sup>CD8<sup>+</sup>CD3<sup>+</sup> T cells pretreatment ( $P = 0.01$ ), after dCRT ( $P = 0.007$ ), and after atezolizumab ( $P = 0.01$ ); for PD-1<sup>+</sup>eT<sub>reg</sub> cells after dCRT ( $P = 0.02$ ) but not pretreatment ( $P = 0.63$ ) nor after atezolizumab ( $P = 0.63$ ); for CTLA-4<sup>+</sup>eT<sub>reg</sub> cells after dCRT ( $P = 0.02$ ) and after atezolizumab ( $P = 0.01$ ) but not pretreatment ( $P = 0.45$ ); and for CD80<sup>+</sup>HLA-DR<sup>+</sup>CD11c<sup>+</sup> cells after atezolizumab ( $P = 0.0004$ ) but not pretreatment ( $P = 0.92$ ) nor after dCRT ( $P = 0.30$ ).

who achieved cCR than in those who did not, and FOXP3<sup>+</sup>CD8<sup>+</sup>CD3<sup>+</sup> T cells were significantly more abundant in patients who did not achieve cCR than in those who did ( $n = 40$ ) (Extended Data Fig. 5c). Accordingly, FCM analysis of PBMCs showed that the proportion of eT<sub>reg</sub> cells among CD45<sup>+</sup> cells pretreatment was significantly higher in patients who did not achieve cCR than in those who did, although the differences in other parameters were insignificant ( $n = 16$ ) (Extended Data Fig. 6a–c). Due to the small sample size of patients whose PBMCs were analyzed by FCM, we further evaluated the results of the complete blood count (CBC) and found no significant differences in the counts of white blood cells (WBCs), neutrophils, lymphocytes or the neutrophil-to-lymphocyte ratio (NLR) before treatment between patients who achieved cCR and those who did not ( $n = 49$ ) (Extended Data Fig. 7).

In conclusion, these data suggest that driver gene mutations, EMT phenotypes with high expression of *MMP1* and *MMP13*, and abundant T<sub>reg</sub> cells in the TME or blood contribute to the evasion of the antitumor response by effector T cells, thereby causing resistance to combination

therapy with dCRT and atezolizumab. These factors may serve as valuable negative predictive biomarkers for this treatment strategy.

#### ESCC analysis after dCRT based on treatment response

We compared the immunological status of patients who did and did not achieve cCR immediately after dCRT and before atezolizumab treatment. Transcriptomic analysis of ESCCs ( $n = 25$ ) immediately after dCRT showed no significant differences between patients who did and did not achieve cCR (Extended Data Fig. 4a–c). FCM analysis of TILs immediately after dCRT and before atezolizumab treatment showed that PD-1 expression in CD8<sup>+</sup> T cells was significantly higher in patients who achieved cCR than in those who did not, whereas PD-1 and CTLA-4 expression in eT<sub>reg</sub> cells were significantly lower in patients who achieved cCR than in those who did not ( $n = 18$ ) (Fig. 4a–c). No significant differences were observed in other parameters evaluated in the FCM analysis of TILs between patients who did and those who did not (Extended Data Fig. 5a,b). FCM analysis of PBMCs ( $n = 17$ ) and

CBC analysis ( $n = 49$ ) performed immediately after dCRT showed no significant differences between patients who did and did not achieve cCR (Extended Data Fig. 6a–c and Extended Data Fig. 7).

These data indicate that the activation of tumor-infiltrating  $eT_{reg}$  cells after dCRT was significantly associated with resistance to atezolizumab treatment. Furthermore, the balance between PD-1 expression in effector T cells and  $eT_{reg}$  cells in the TME immediately before atezolizumab treatment predicted the efficacy of atezolizumab<sup>39</sup>.

### Residual ESCC characteristics after combination therapy

We evaluated the genomic and immunological features of ESCCs after treatment to investigate the resistance mechanisms after combination therapy with dCRT and sequential atezolizumab. DEG analysis of ESCCs after atezolizumab treatment was performed to identify genes significantly associated with non-cCR (Fig. 5a). We identified *IL1A* and *IL1B* among the DEGs in the residual ESCCs of patients who did not achieve cCR ( $n = 25$ ) (Fig. 5a and Extended Data Fig. 8a). During the treatment course, *IL1A* gene expression was not significantly elevated in patients who achieved cCR or in those who did not ( $n = 25$ ) (Fig. 5b). In contrast, *IL1B* expression was significantly upregulated only in patients who did not achieve cCR ( $n = 25$ ) (Fig. 5c).

IL-1 $\beta$  induces myeloid-derived suppressor cells (MDSCs) in the TME<sup>40</sup>. Furthermore, upon irradiation, IL-1 polarizes cancer-associated fibroblasts (CAFs) toward an inflammatory phenotype and triggers oxidative DNA damage, thereby predisposing inflammatory CAFs (iCAFs) to p53-mediated therapy-induced senescence, resulting in treatment resistance<sup>41</sup>. Consistent with this, GSEA showed that in patients who did not achieve cCR, IL-1R-related gene expression, granulocyte-related gene expression, iCAF signature and CAF signature were enriched in residual ESCCs immediately after dCRT compared to specimens before treatment (Fig. 5d). When comparing the gene expression of specimens from patients who achieved cCR with those who did not after atezolizumab treatment, IL-1R-related gene expression, granulocyte-related gene expression and iCAF and CAF signatures were enriched in the ESCCs of patients who did not achieve cCR (Extended Data Fig. 8b). Furthermore, our transcriptomic analysis showed that the MDSC-related ssGSEA scores (MDSC\_ShirleyLiu scores) of patients who did not achieve cCR were significantly higher than those of patients who achieved cCR after atezolizumab treatment ( $n = 25$ ) (Extended Data Fig. 8c). We also compared the gene expression of immune-related molecules (Extended Data Figs. 4a and 5c) and found that the expression of *NECTIN2* and *PVR*, which are major ligands of TIGIT<sup>42</sup>, was significantly higher in patients who did not achieve cCR than in those who achieved cCR after atezolizumab treatment (Extended Data Fig. 4b). Additionally, we analyzed the FCM data from TILs after atezolizumab treatment ( $n = 18$ ) (Fig. 4a–e and Extended Data Fig. 5a,b). PD-1 expression in CD8<sup>+</sup> T cells from patients who achieved cCR was significantly higher than that in CD8<sup>+</sup> T cells from patients who did not achieve cCR (Fig. 4a), whereas CTLA-4 expression in  $eT_{reg}$  cells from patients who achieved cCR was significantly lower

than that in  $eT_{reg}$  cells from patients who did not achieve cCR (Fig. 4c). The expression of CD80 in the APCs of patients who achieved cCR was higher than that in those who did not, although this difference was not significant (Fig. 4d and Extended Data Fig. 5b). Consistent with the FCM data, GSEA showed that CTLA-4-related gene expression increased in patients who did not achieve cCR during the treatment course (Fig. 5d and Extended Data Fig. 8d). These data aligned with a previous report suggesting that IL-1 increases the suppressive function of  $T_{reg}$  cells in the inflammatory TME and that intratumoral IL1R1<sup>+</sup>  $T_{reg}$  cells are highly activated<sup>43</sup>. Additionally, although no significant differences were found in the FCM analysis of PBMCs, the CBC analysis determined that the neutrophil counts and NLR post-atezolizumab treatment were significantly higher in patients who did not achieve cCR than in those who did (Extended Data Fig. 7). Based on the CBC and tumor tissue sample analysis results, residual ESCCs refractory to combination therapy with dCRT and atezolizumab may cause systemic inflammatory responses in some patients.

Collectively, we suggest that after sequential combination therapy with dCRT and atezolizumab, residual ESCCs could employ an immunosuppressive mechanism in  $eT_{reg}$  cells involving the recruitment of iCAFs and MDSCs and upregulation of CTLA-4 expression via IL-1 $\beta$  (Extended Data Fig. 8e). These insights into resistance mechanisms may facilitate the development of novel and effective treatment strategies for ESCC.

### Discussion

This phase II proof-of-concept clinical trial evaluated the safety, efficacy and predictive biomarkers of definitive CRT followed by the anti-PD-L1 antibody atezolizumab in patients with unresectable locally advanced ESCC. We selected cases of purely unresectable locally advanced ESCC, mainly clinical stage IVA or IVB, and observed a promising 42.1% cCR rate of 65.8% 1-year OS rate. The Chinese phase II EC-CRT-001 trial indicated a 62% cCR rate and a 78.4% 1-year OS rate in patients treated concurrently with the anti-PD-1 antibody toripalimab; however, only 62% of inoperable patients and 38% of patients with clinical stage IVA were included because patients who refused radical surgery or had cervical esophageal cancer were eligible<sup>44</sup>.

The synergistic efficacy of combination treatment with CRT followed by atezolizumab was strongly suggested by our translational analysis and the detected predictive signals were potential biomarkers. Moreover, because CRT is a standard treatment option for patients with early stage locally advanced ESCC, the application of sequential combinations of CRT and atezolizumab is potentially expandable to patients with ESCC at all stages and the results of our trial may guide standard ESCC treatment modifications.

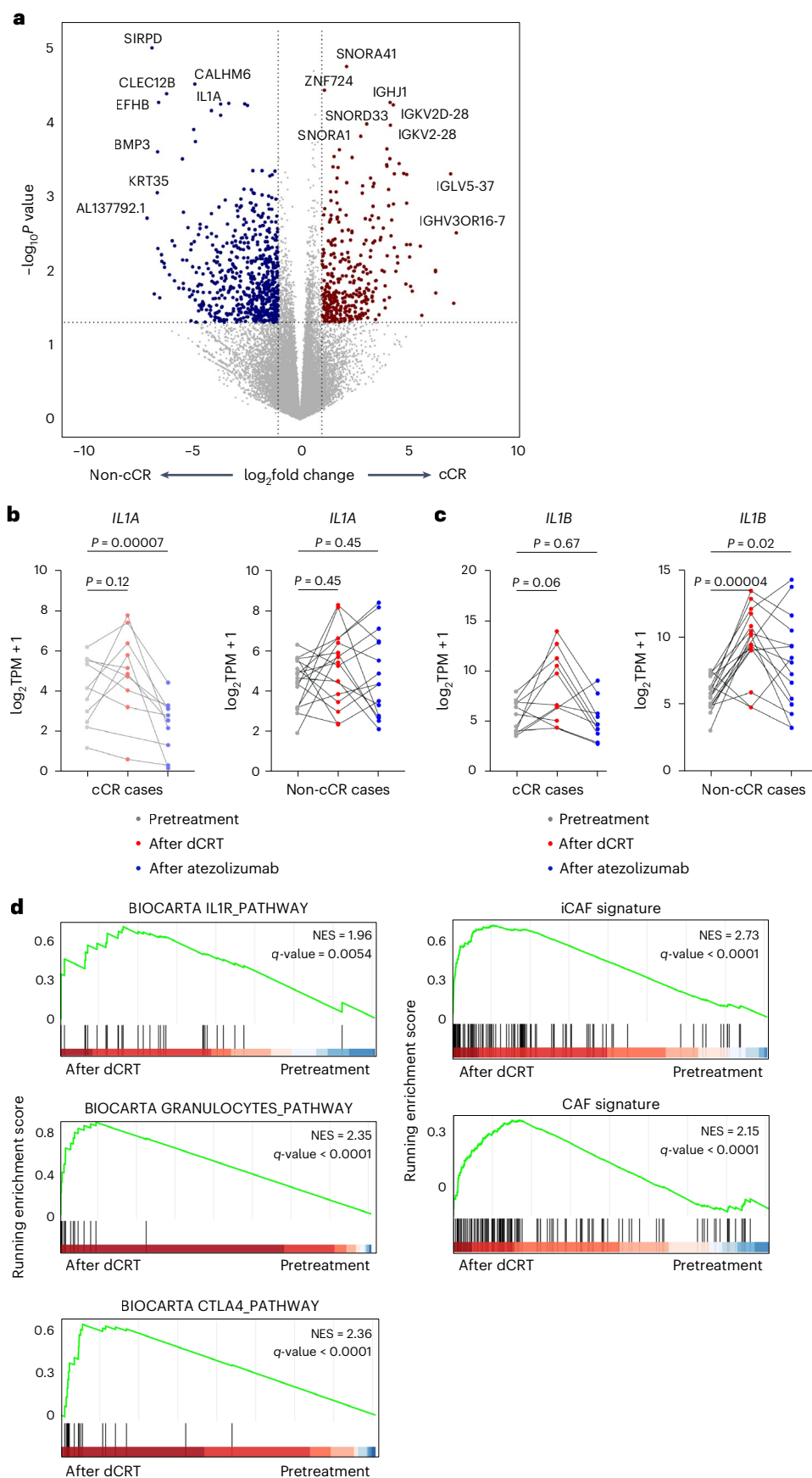
Although preclinical studies have shown that CRT improves the therapeutic effect of ICI therapy<sup>15–17,45</sup>, concurrent CRT and ICI therapy increases the risk of serious adverse events (AEs)<sup>46</sup> and may decrease the number of immune-activated lymphocytes from adjacent lymph nodes. This clinical trial involved dCRT followed by sequential atezolizumab treatment. In this study, dCRT not only killed tumor cells, but

### Fig. 5 | Transcriptomic analysis showed that IL-1R-related pathways are related to resistance after combination therapy with dCRT and atezolizumab.

**a**, Volcano plots analyzing enriched differential genes between non-cCR ESCC and cCR esophageal cancer samples after combination therapy are shown. Red, patients who achieved cCR (cCR cases); blue, patients who did not achieve cCR (non-cCR cases). *P* values were calculated using the likelihood ratio test. **b**, *IL1A* expression in the ESCCs of cCR cases (left) and non-cCR cases (right) during treatment (pretreatment (cCR,  $n = 11$  patients; non-cCR,  $n = 17$  patients), after dCRT (cCR,  $n = 10$  patients; non-cCR,  $n = 15$  patients) and after atezolizumab treatment (cCR,  $n = 10$  patients; non-cCR,  $n = 15$  patients)) was evaluated. Summaries of the TPM values of *IL1A* in the ESCCs of cCR cases (left) and non-cCR cases (right) are shown. **c**, *IL1B* expression in the ESCCs of cCR cases (left) and non-cCR cases (right) during treatment (pretreatment (cCR,  $n = 11$  patients; non-cCR,  $n = 17$  patients), after dCRT (cCR,  $n = 10$  patients; non-cCR,  $n = 15$  patients)

and after atezolizumab treatment (cCR,  $n = 10$  patients; non-cCR,  $n = 15$  patients)) was evaluated. Summaries of the TPM values of *IL1B* in the ESCCs of cCR cases (left) and non-cCR cases (right) are shown. Gray, pretreatment; red, after dCRT; blue, after atezolizumab (**b,c**). *P* values were calculated by one-way ANOVA. For multiple comparisons, Holm–Sidak’s test was performed. Differences with  $P \leq 0.05$  were considered statistically significant. Significant differences were found in *IL1A* for cCR cases ( $P = 0.00007$ ) but not non-cCR cases ( $P = 0.45$ ) and in *IL1B* for non-cCR cases ( $P = 0.02$ ) but not cCR cases ( $P = 0.67$ ). **d**, Gene expression in ESCCs after dCRT was compared to that in ESCCs before treatment by performing GSEA with the indicated gene sets in non-cCR cases. Plots of the enrichment of IL-1R pathway-related genes (left top), granulocyte pathway-related genes (left middle), CTLA-4 pathway-related genes, the iCAF signature (right top) and the CAF signature (right bottom) are shown.





also increased the response to IFNs via enhancement of the cGAS–STING and/or RIG-I pathways<sup>16,17,20–23</sup>, resulting in the activation of APCs and effector T cells, thereby inducing an antitumor immune response. In contrast, our analysis of ESCCs during treatment showed that the expression of suppressive immune-checkpoint molecules, such as PD-L1, in tumor tissues was upregulated after dCRT, as shown in previous studies<sup>15–17</sup>. In addition, dCRT increased the expression of CD80, CD86 and PD-L1 in APCs, which is consistent with preclinical studies<sup>15,47</sup>. These results strongly support our hypothesis that PD-L1 inhibition after the completion of dCRT therapy can further improve the antitumor immune response and, thus, the therapeutic response.

In this study, we evaluated whether TMB and PD-L1 expression are predictive biomarkers of dCRT followed by sequential atezolizumab treatment for ESCC; however, neither TMB nor PD-L1 expression correlated with clinical outcomes. We have previously reported that the balance of PD-1 expression between CD8<sup>+</sup> T cells and T<sub>reg</sub> cells in the TME is a promising biomarker for PD-1 blockade<sup>39</sup>. Analysis of patient samples pre-combination treatment with dCRT and sequential atezolizumab revealed high and low infiltration of PD-1<sup>+</sup>CD8<sup>+</sup> T cells and T<sub>reg</sub> cells in the TME, respectively. Additionally, the low proportion of eT<sub>reg</sub> cells among CD45<sup>+</sup> cells in PBMCs was associated with a therapeutic response. Furthermore, analysis of specimens immediately after dCRT treatment and before atezolizumab treatment revealed that PD-1 expression in tumor-infiltrating CD8<sup>+</sup> T cells was significantly positively correlated with the therapeutic response, whereas PD-1 expression in tumor-infiltrating T<sub>reg</sub> cells was significantly negatively correlated with the therapeutic response, consistent with the results of our previous study<sup>29,39,48</sup>. In some patients in the current study, PD-1 expression in eT<sub>reg</sub> cells in the TME was elevated after dCRT and PD-1 blockade enhanced suppressive activity, including increased CTLA-4 expression and, thus, dampened antitumor immune responses. This suggests the importance of combining T<sub>reg</sub> cell-targeted therapies, including anti-CTLA-4, anti-CD25 or anti-CCR8 antibodies<sup>11,49,50</sup>.

We performed genomic analysis of treatment-resistant ESCCs and found that they harbored genetic abnormalities, including *EGFR*, *PIK3CA*, *PTEN* or *KEAP1* mutations or *MYC* amplification, before treatment. Previous studies have shown that driver gene mutations in cancers are associated with resistance to immunotherapy<sup>28–33</sup>. Our transcriptome analysis of ESCCs before treatment revealed that the ESCCs exhibiting the EMT phenotype with high expressions of *MMPI1* and *MMPI3* and/or upregulated TGF- $\beta$  signaling were likely to be resistant to sequential combination treatment with dCRT and atezolizumab. These results corroborate those of previous studies suggesting that cancers exhibiting the EMT phenotype are resistant to both cancer immunotherapy and CRT<sup>34,35,38</sup>. High expression levels of *MMPI1* and *MMPI3* in tumor samples can be used as negative predictive biomarkers.

Further analysis of the post-treatment samples revealed several possible resistance mechanisms. First, in patients who showed resistance to this combination of dCRT and sequential atezolizumab, the gene signature of the IL-1R pathway was upregulated after combination with dCRT and sequential atezolizumab, possibly causing systemic inflammatory responses. A previous report suggested that after irradiation, IL-1 not only polarizes CAFs toward the inflammatory phenotype, but also triggers oxidative DNA damage, resulting in chemoradiotherapy resistance<sup>41</sup>. Furthermore, IL-1 $\beta$  reportedly induces MDSCs in the TME<sup>40</sup>, causing resistance to cancer immunotherapy<sup>51</sup>. In this study, abundant IL-1 $\beta$  in patients who did not achieve cCR could possibly induce MDSCs in the TME after dCRT, suppressing antitumor immune responses. Second, CTLA-4 expression in eT<sub>reg</sub> cells in the TME increased, possibly inhibiting antitumor immune responses by downregulating CD80/CD86 (ref. 52). IL-1 strengthens the suppressive activities of T<sub>reg</sub> cells in the inflammatory microenvironment<sup>43</sup>.

Finally, high expression of *PVR* and *NECTIN2* may inhibit effector T cell activation via the TIGIT pathway<sup>42</sup>, resulting in resistance to combination therapy. The addition of inhibitors of IL-1R<sup>41</sup>, CTLA-4

(refs. 53,54) or TIGIT<sup>55</sup> in combination with dCRT and sequential atezolizumab may be considered for patients with ESCC who are refractory to this treatment. Further clinical trials are warranted to develop these novel therapies. The randomized phase III SKYSCRAPER-07 trial (NCT04543617) comparing 1 year of atezolizumab plus anti-TIGIT antibody (tiragolumab), atezolizumab plus placebo, and double placebo after platinum-based dCRT in a 1:1:1 manner in patients with unresectable locally advanced ESCC is ongoing. This trial will confirm the clinical benefits of anti-PD-L1  $\pm$  anti-TIGIT blockade after dCRT for unresectable locally advanced ESCC.

Our study has several limitations. This was a nonrandomized phase II study with a relatively small sample size. Although promising cCR and 1-year PFS rates have been reported, long-term survival data have not been reported. To confirm the survival benefits of the sequential combination of dCRT and atezolizumab, the results of the randomized phase III SKYSCRAPER-07 trial are essential.

In conclusion, atezolizumab monotherapy following dCRT resulted in a promising cCR rate and may lead to long-term survival without additional safety concerns. Tumor-infiltrating PD-1<sup>+</sup>CD8<sup>+</sup> T cells detected by FMC and/or mIHC can serve as biomarkers of cCR. Further studies are required to generalize our findings to all stages of ESCC.

## Methods

### Ethical approval and consent to participate

This study was conducted in accordance with the guidelines for Good Clinical Practice of the International Council on Harmonization of Technical Requirements for Registration of Pharmaceuticals for Human Use and the Ethical Guidelines for Medical and Health Research Involving Human Subjects. The REporting recommendations for tumor MARKer prognostic studies (REMARK)<sup>56</sup> and the Consolidated Standards of Reporting Trials (CONSORT)<sup>57</sup> were followed. This study was approved by the ethics committee of each participating institution (National Cancer Center Institutional Review Board, Aichi Cancer Center Institutional Review Board, Saitama Cancer Center Review Board, Shizuoka Cancer Center Review Board and Cancer Institute Hospital of the Japanese Foundation for Cancer Research Review Board). All patients provided written informed consent before enrollment.

### Study design and treatments

The EPOC1802 TENERGY trial is a multicenter phase II study that assessed the safety and efficacy of sequential combination therapy with atezolizumab following 5-FU plus cisplatin-based chemoradiotherapy (60 Gy/30 fractions without prophylactic irradiation) in patients with unresectable locally advanced ESCC without distant metastasis. All patients who met the eligibility criteria were registered sequentially. The study was registered with the University Hospital Medical Information Network (clinical trial information no. UMIN000034373).

Three-dimensional conformal radiotherapy was administered weekly for five consecutive days with a target dose of 60 Gy in 30 fractions. The gross tumor volume (GTV) was defined as the primary tumor and positive lymph nodes. The clinical target volume (CTV) was defined as the primary GTV plus a 2 cm proximal and distal margin, and the nodal CTV was equal to the corresponding GTV. For recurrent lesions, the CTV was identical to the GTV. The planning target volume was defined as the primary, nodal and recurrence CTV plus a 0.5–2 cm proximal and distal margin as well as a radial margin of 0.5–1.0 cm. Dose constraints to the organs at risk were as follows: lung V20 (percentage of the total lung volume receiving  $\geq 20$  Gy) <35%, lung V5 (percentage of the total lung volume receiving  $\geq 5$  Gy) <65%, mean heart dose <40 Gy and maximum spinal cord dose <45 Gy, spinal cord V45 (volume of the spinal cord receiving  $\geq 45$  Gy). Quality assurance for radiotherapy includes target volume determination, volume to be irradiated, dose and fractionation, and dosimetric criteria for targets and organs at risk, which must align with the trial protocol. Normal tissue dose constraints were based on the QUANTEC criteria. Radiation plans were collected

and subjected to a centralized review to assess compliance with protocol requirements pretreatment.

We enrolled patients with primary locally advanced ESCC in the primary cohort ( $n = 40$ ) and those with locoregionally recurrent ESCC after surgical resection in the exploratory cohort ( $n = 10$ ). Seven institutions including the National Cancer Center Hospital East, National Cancer Center Hospital, Saitama Cancer Center, Cancer Institute Hospital of the Japanese Foundation for Cancer Research, Shizuoka Cancer Center, and Aichi Cancer Center participated in this study. The enrollment period was from December 2018 to March 2021 and the study was completed in January 2022.

The main inclusion criteria were histologically confirmed primary ESCC, an unresectable tumor with T4b (a tumor invading other adjacent structures such as the aorta, vertebral body or trachea) and/or regional lymph node and/or supraclavicular lymph node invasion of adjacent structures other than the esophagus, treatment with two cycles of CDDP ( $70 \text{ mg m}^{-2}$ ) on day 1 plus 5-FU ( $700 \text{ mg m}^{-2}$ ) on days 1–4 every 4 weeks and 60 Gy/30 fractions of radiotherapy, and the absence of esophageal perforation, esophagotracheal fistula, esophagomediastinal fistula, bleeding from arterial invasion or respiratory stenosis when CRT was completed (Supplementary Table 6). Clinical stage was assessed by members of a multidisciplinary team according to the Eighth TNM staging system of the American Joint Committee on Cancer<sup>58</sup>.

Both chemotherapy and radiation are highly qualified based on quality assurance and quality control programs. The study treatment was initiated within 6 weeks of CRT completion. Patients received 1,200 mg atezolizumab every 3 weeks for 12 months (maximum of 17 doses) or until disease progression, patient withdrawal, investigator's decision, pregnancy or unacceptable toxicity, whichever occurred first. The study protocol is included in the Supplementary Information.

### End points and assessments

The primary end point was cCR rate, as determined by the investigator's assessment of the primary locally advanced ESCC cohort. The secondary end points were the cCR rate determined by an investigator's assessment in the locoregionally recurrent ESCC cohort. Moreover, we assessed the cCR rate determined by central assessment, overall response rate determined by the investigator's assessment, PFS, OS and the incidence of AEs in both cohorts as the secondary end points<sup>59</sup>.

Complete response (CR) was determined by both computed tomography (CT) and endoscopy based on the Response Evaluation Criteria in Solid Tumors v.1.1, with modifications, and the Japanese Classification of Esophageal Cancer (11th edition). CR was defined as absence of erosive changes with irregularities, ulcerative lesions, obvious elevation (including submucosal mass elevations) or histopathological malignancy. Both CT and endoscopic examinations were performed every 4 weeks until CR, following confirmation of CR after more than 4 weeks and every 12 weeks thereafter<sup>59</sup>. Before atezolizumab therapy, we performed CT and endoscopy, with no patient achieving CR immediately after CRT.

PFS was defined as the period from the date of enrollment to the date of disease progression or death from any cause, whichever occurred first. OS was defined as the period from the date of enrollment to death from any cause. We assessed AEs according to the Common Terminology Criteria for Adverse Events v.4.0 (ref. 59).

Clinical data were collected using Medidata Rave (v.2015.1.1) and Medidata Classic Rave (v.2018.2.0). The data center of the Clinical Research Support Office, National Cancer Center Hospital East (NCCHE-OCRS) confirmed patient eligibility. Data collection, analyses and interpretation were performed by the NCCHE-OCRS.

### Complete blood count

The CBCs, which included WBCs, RBCs and platelet counts and the concentrations of hemoglobin, hematocrit and WBC differentials, were determined using automated hematology analyzers at each institute.

### PD-L1 evaluation and biomarker analyses

Serial biopsies from the primary site and blood collections were performed at three time points ( $<4$  weeks before treatment,  $<6$  weeks after dCRT and  $4 \pm 2$  weeks after the first atezolizumab dose). PD-L1 expression in the tumor cells was evaluated using the VENTANA PD-L1 (SP263) assay. Using the collected samples, we investigated the biomarkers for efficacy or resistance to the study treatments. We collected available samples, including frozen tumor tissue specimens, formalin-fixed paraffin-embedded tumor tissue specimens and frozen blood specimens, from patients enrolled in this study. We analyzed WES and RNA-seq data, TMB, phenotype of immune-competent cells using immunohistochemistry and PD-L1 status. Fresh tumor tissues and blood specimens were obtained from patients enrolled in the National Cancer Center Hospital East ( $n = 18$ ). The fresh specimens were processed as described in the following sections and subjected to FCM.

### WES

DNA and/or RNA were extracted from frozen tumors or blood samples at each time point using an AllPrep DNA/RNA Mini kit (QIAGEN). WES was performed on 27 patients before treatment. Exome library construction was performed using the SureSelect V6-Post kit (Agilent Technology) as described in the manufacturer's protocol. The adaptor-ligated fragments were amplified by PCR. Paired-end sequencing (151 bp) was performed using HiSeq X (Illumina). For exome analyses, paired-end sequencing reads with masked nucleotides and a quality score of  $<20$  were aligned to hg38 using BWA-MEM (<http://bio-bwa.sourceforge.net/>) and Bowtie2 (<http://bowtie-bio.sourceforge.net/bowtie2/index.shtml>). Both synonymous and nonsynonymous somatic mutations were identified using our inhouse caller and two publicly available mutation callers: the Genome Analysis Toolkit (<https://gatk.broadinstitute.org/hc/en-us>), MuTect2 and VarScan2 (<http://varscan.sourceforge.net/>). Mutations were discarded if any of the following criteria were met: a total read number of  $<100$ , a variant allele frequency in the tumor samples of  $<0.05$ , a mutant read number in the germline control samples of  $>2$  mutations detected in only one strand of the genome or a variant present in normal human genomes in either the 1000 Genomes Project dataset (<https://www.internationalgenome.org/>) or our inhouse database. Gene mutations were annotated using SnpEff (<http://snpeff.sourceforge.net>).

### RNA-seq analysis

RNA-seq libraries for paired patient tumor samples ( $n = 28$ ) during treatment were prepared using the TruSeq RNA Access Library Prep kit and 101 bp paired-end sequencing was performed using the Illumina platform at MACROGEN. The raw FASTQ read sequences were trimmed and filtered using Trim Galore (v.0.6.5), to remove low-quality bases. Adaptor sequences and reads mapped to rRNA genes were removed using bowtie2 (v.2.4.1). The filtered FASTQs were then aligned to the human genome (GRCh38) using STAR (v.2.7.3a). Gene expression values were calculated as either counts or transcripts per million (TPM) using Stringtie (v.2.2.1), with GENCODE (v.34) gene annotation. Normalization and differential expression analyses were performed using DESeq2 with the count data.

### GSEA and ssGSEA

GSEA of gene expression data from RNA-seq was performed using clusterProfiler (v.4.4.4)<sup>60</sup>. The following gene signatures were analyzed: HALLMARK and C2 curated gene sets from MSigDB<sup>25,61</sup>, inflammatory cancer-associated fibroblast (iCAF) signature<sup>41</sup>, and CAF signature<sup>62</sup>. GSEA plots were generated using Enrichment Plot (v.1.16.2). ssGSEA was conducted using GSVA (v.1.44.5)<sup>63</sup> with TPM profiles. The immunological gene signature of Dummer et al.<sup>64</sup> was analyzed. ssGSEA scores were normalized using Z-scaling. These analyses were performed using R software (v.4.2.2).



### Multicolor FCM analysis

Paired TILs ( $n = 19$ ) and PBMCs ( $n = 18$ ) were collected from patients treated at the National Cancer Center Hospital East. To collect TILs, tumor tissues were minced and treated within 72 h after biopsy with a new TIL preparation protocol using newly optimized tissue preservation reagent (tumor tissue dissociation reagent; TTPR) and TIL-isolation reagent (tumor tissue dissociation reagent; TTDR) co-developed with BD Biosciences (see details in PCT/JP2020/005991) as previously described, and the prepared cells (TILs) were subjected to analyses<sup>65</sup>. In brief, fresh tumor specimens were placed into a tube filled with TTPR solution at 2–8 °C for  $\leq 72$  h. After preservation, tumor specimens were cut into small pieces (approximately 0.5–1.0 mm per side) using scissors in a tube. TTDR was added to the tubes. The cap was tightly closed and the tube was incubated at 20–25 °C for 15 min on the nutator. After incubation, a cold stop buffer was added to the tubes. The cell suspension was passed through a cell strainer and centrifuged to isolate tumor-infiltrating immune cells. The PBMCs were isolated by density gradient centrifugation using Ficoll-Paque (GE Healthcare). FCM staining and analysis were performed as previously described. The antibodies used for FCM analyses are summarized in Supplementary Table 7. To evaluate the influence of atezolizumab treatment on the stainability of the anti-PD-L1 antibody, PBMC samples were incubated with or without atezolizumab (final concentration of 200  $\mu\text{g ml}^{-1}$ ) at 37 °C for 20 min before staining with FCM antibodies. Cells (PBMCs and TILs) were washed using a washing solution and stained with surface antibodies, including the anti-CTLA-4 antibody (1:50 dilution). Intracellular staining of some molecules, including FOXP3, was performed with the corresponding antibodies (for example, anti-FOXP3 monoclonal antibody) and the Foxp3/Transcription Factor Staining Buffer Set (Thermo Fisher Scientific), according to the manufacturer's instructions. After washing, the cells were analyzed using a FACSymphony (BD Biosciences) and FlowJo software v.10.8.1 (TreeStar). The gating strategy used in this study is shown in Extended Data Fig. 9.

### mIHC

mIHC was performed on tumor tissues from 40 patients. Optimized mIHC was performed using an Opal six-color tyramide signaling amplification kit (Akoya Biosciences). Cells were stained with antibodies against CD3 (clone SP7, ab16669, Abcam, 1:200 dilution), CD8 (clone C8/144B, M710301-2, Agilent, 1:200 dilution), FOXP3 (clone 236A/E7, ab96048, Abcam, 1:100 dilution), cytokeratin (clone AE1+AE3, ARG56129, Arigo Biolaboratories, 1:200 dilution) and PD-1 (clone EPR4877(2), ab137132, Abcam, 1:50 dilution). Fluorescence signals were captured with the fluorophores Opal 520, Opal 540, Opal 570, Opal 620, Opal 650 and Opal 690. Multiplex-stained slides were obtained using the Vectra Polaris Quantitative Pathology Imaging System (PerkinElmer). The images were analyzed using inForm (v.2.4.4) image analysis software (PerkinElmer) and Spotfire software (v.12.2; TIBCO Software). Whole-slide images were analyzed using IA software (HALO v.2.3; Indica Labs). Slides were manually annotated to remove tissue artifacts (for example, folds, air bubbles and fluorescent precipitates), and segmentation and markup of individual cells were performed, reviewed and scored by two pathologists using the Indica Labs-HighPlex FL module.

### Statistical analysis for translational analysis

Data analyses were performed using GraphPad Prism v.9 (GraphPad Software). Microsoft Excel 2016 (Microsoft Corporation) was used for data collection. ssGSEA scores, TPM, FCM analysis parameters and mIHC parameters were calculated using a paired one-way analysis of variance or an unpaired two-tailed  $t$ -test. The Holm–Sidak test was performed for multiple comparisons. The differences with  $P \leq 0.05$  were considered significant. The data distribution was assumed to be normal; however, this was not formally tested.

### Statistics and reproducibility

The reported cCR rates range from 11 to 25%. In the present study, we estimated the rate of cCR threshold at 20%, based on discussions with investigators and statisticians, and regulatory science consultation by healthcare authorities. Therefore, we calculated the sample size of the primary locally advanced ESCC cohort at 38 with a cCR of 40% deemed promising and one of 20% deemed unacceptable (one-sided  $\alpha$ , 0.05;  $\beta$ , 0.2). Using this calculation, we included a maximum of 40 patients with locally advanced primary ESCC in the primary cohort. We further set the planned sample size of the exploratory cohort with postoperative locoregionally recurrent ESCC at a maximum of ten patients in an exploratory manner. The cCR was determined by the investigator's assessment and the CI was estimated using the exact binomial method. The primary end point was analyzed in the first 38 consecutive patients who were deemed eligible and received the protocol treatment at least once. Results were considered statistically significant for more than 13 confirmed cases of CR. PFS and OS were estimated using the Kaplan–Meier method. Statistical analyses were performed using the SAS software (v.9.4; SAS Institute). The data cutoff date for the analyses was 4 March 2022. No data were excluded from the analyses and the experiments were not randomized. The investigators were not blinded to the allocation during the experiments or outcome assessment. Data collection and analysis were conducted without blinding to the conditions of the experiments. As this was a single-arm phase II study, specimens were collected from patients only once at each time point and the volume of each specimen collected was small. Therefore, it was impossible to replicate the validation experiments.

### Reporting summary

Further information on research design is available in the Nature Portfolio Reporting Summary linked to this article.

### Data availability

All exome and transcriptome data have been deposited in the NBDC Human Database (<https://humandbs.dbcls.jp/en/hum0294-v1>). The accession numbers are JGAS000708 for the study and JGAD000841 for the dataset. These data are subject to restricted access and available only to researchers who have submitted a data usage application and have had their application approved. If one wishes to use this data, one must submit a data usage application through the application system. The procedure is described at <https://humandbs.dbcls.jp/en/data-use>. Use of the data is subject to the NBDC Human Data Sharing Guidelines and the NBDC Human Data Handling Security Guidelines (for data users). The hg38 dataset was accessed from [https://www.encodegenes.org/human/release\\_34.html](https://www.encodegenes.org/human/release_34.html). Source data for Figs. 2–5 and Extended Data Figs. 2–9 are provided as Source Data files. All other data supporting the findings of this study are available from the corresponding author upon reasonable request. Source data are provided with this paper.

### Code availability

All codes used in the analyses described in this study were based on existing tools and software, and no custom software, programs or scripts were used. We have uploaded the code used in the analyses to GitHub, accessible at [https://github.com/CancerImmunologyNCC/Bando\\_etal\\_2024\\_RNAseq](https://github.com/CancerImmunologyNCC/Bando_etal_2024_RNAseq).

### References

1. Sung, H. et al. Global Cancer Statistics 2020: GLOBOCAN estimates of incidence and mortality worldwide for 36 cancers in 185 countries. *CA Cancer J. Clin.* **71**, 209–249 (2021).
2. Tachimori, Y. et al. Comprehensive registry of esophageal cancer in Japan, 2012. *Esophagus* **16**, 221–245 (2019).
3. Obermannova, R. et al. Esophageal cancer: ESMO Clinical Practice Guideline for diagnosis, treatment and follow-up. *Ann. Oncol.* **33**, 992–1004 (2022).



4. Kitagawa, Y. et al. Esophageal cancer practice guidelines 2017 edited by the Japan Esophageal Society: part 1. *Esophagus* **16**, 1–24 (2019).
5. Ajani, J. A. et al. Esophageal and esophagogastric junction cancers, Version 2.2023, NCCN Clinical Practice Guidelines in Oncology. *J. Natl Compr. Canc. Netw.* <https://doi.org/10.6004/jnccn.2023.0019> (2023).
6. Ishida, K., Ando, N., Yamamoto, S., Ide, H. & Shinoda, M. Phase II study of cisplatin and 5-fluorouracil with concurrent radiotherapy in advanced squamous cell carcinoma of the esophagus: a Japan Esophageal Oncology Group (JEOG)/Japan Clinical Oncology Group trial (JCOG9516). *Jpn J. Clin. Oncol.* **34**, 615–619 (2004).
7. Ohtsu, A. et al. Definitive chemoradiotherapy for T4 and/or M1 lymph node squamous cell carcinoma of the esophagus. *J. Clin. Oncol.* **17**, 2915–2921 (1999).
8. Shinoda, M. et al. Randomized study of low-dose versus standard-dose chemoradiotherapy for unresectable esophageal squamous cell carcinoma (JCOG0303). *Cancer Sci.* **106**, 407–412 (2015).
9. Habu, T. et al. Complete response to definitive chemoradiotherapy in unresectable locally advanced esophageal squamous cell carcinoma. *Esophagus* **20**, 533–540 (2023).
10. Herskovic, A. et al. Combined chemotherapy and radiotherapy compared with radiotherapy alone in patients with cancer of the esophagus. *N. Engl. J. Med.* **326**, 1593–1598 (1992).
11. Doki, Y. et al. Nivolumab combination therapy in advanced esophageal squamous-cell carcinoma. *N. Engl. J. Med.* **386**, 449–462 (2022).
12. Sun, J. M. et al. Pembrolizumab plus chemotherapy versus chemotherapy alone for first-line treatment of advanced oesophageal cancer (KEYNOTE-590): a randomised, placebo-controlled, phase 3 study. *Lancet* **398**, 759–771 (2021).
13. Kelly, R. J. et al. Adjuvant nivolumab in resected esophageal or gastroesophageal junction cancer. *N. Engl. J. Med.* **384**, 1191–1203 (2021).
14. Shah, M. A., Hofstetter, W. L. & Kennedy, E. B. Immunotherapy in patients with locally advanced esophageal carcinoma: ASCO treatment of locally advanced esophageal carcinoma guideline rapid recommendation update. *J. Clin. Oncol.* <https://doi.org/10.1200/jco.21.01831> (2021).
15. Deng, L. et al. Irradiation and anti-PD-L1 treatment synergistically promote antitumor immunity in mice. *J. Clin. Invest.* **124**, 687–695 (2014).
16. Dovedi, S. J. et al. Acquired resistance to fractionated radiotherapy can be overcome by concurrent PD-L1 blockade. *Cancer Res.* **74**, 5458–5468 (2014).
17. Zhang, P., Su, D. M., Liang, M. & Fu, J. Chemopreventive agents induce programmed death-1-ligand 1 (PD-L1) surface expression in breast cancer cells and promote PD-L1-mediated T cell apoptosis. *Mol. Immunol.* **45**, 1470–1476 (2008).
18. Antonia, S. J. et al. Durvalumab after chemoradiotherapy in stage III non-small-cell lung cancer. *N. Engl. J. Med.* **377**, 1919–1929 (2017).
19. Antonia, S. J. et al. Overall survival with durvalumab after chemoradiotherapy in stage III NSCLC. *N. Engl. J. Med.* **379**, 2342–2350 (2018).
20. Deng, L. et al. STING-dependent cytosolic DNA sensing promotes radiation-induced type I interferon-dependent antitumor immunity in immunogenic tumors. *Immunity* **41**, 843–852 (2014).
21. Mackenzie, K. J. et al. cGAS surveillance of micronuclei links genome instability to innate immunity. *Nature* **548**, 461–465 (2017).
22. Ranoa, D. R. et al. Cancer therapies activate RIG-I-like receptor pathway through endogenous non-coding RNAs. *Oncotarget* **7**, 26496–26515 (2016).
23. Tigano, M., Vargas, D. C., Tremblay-Belzile, S., Fu, Y. & Sfeir, A. Nuclear sensing of breaks in mitochondrial DNA enhances immune surveillance. *Nature* **591**, 477–481 (2021).
24. Sharabi, A. B. et al. Stereotactic radiation therapy augments antigen-specific PD-1-mediated antitumor immune responses via cross-presentation of tumor antigen. *Cancer Immunol. Res.* **3**, 345–355 (2015).
25. Subramanian, A. et al. Gene set enrichment analysis: a knowledge-based approach for interpreting genome-wide expression profiles. *Proc. Natl Acad. Sci. USA* **102**, 15545–15550 (2005).
26. Miyara, M. et al. Functional delineation and differentiation dynamics of human CD4<sup>+</sup> T cells expressing the FoxP3 transcription factor. *Immunity* **30**, 899–911 (2009).
27. Zehn, D., Thimme, R., Lugli, E., de Almeida, G. P. & Oxenius, A. ‘Stem-like’ precursors are the fount to sustain persistent CD8(+) T cell responses. *Nat. Immunol.* **23**, 836–847 (2022).
28. Topper, M. J. et al. Epigenetic therapy ties MYC depletion to reversing immune evasion and treating lung cancer. *Cell* **171**, 1284–1300.e1221 (2017).
29. Kumagai, S. et al. Lactic acid promotes PD-1 expression in regulatory T cells in highly glycolytic tumor microenvironments. *Cancer Cell* <https://doi.org/10.1016/j.ccell.2022.01.001> (2022).
30. Sugiyama, E. et al. Blockade of EGFR improves responsiveness to PD-1 blockade in EGFR-mutated non-small cell lung cancer. *Sci. Immunol.* <https://doi.org/10.1126/sciimmunol.aav3937> (2020).
31. Peng, W. et al. Loss of PTEN promotes resistance to T cell-mediated immunotherapy. *Cancer Discov.* **6**, 202–216 (2016).
32. Marzio, A. et al. EMSY inhibits homologous recombination repair and the interferon response, promoting lung cancer immune evasion. *Cell* **185**, 169–183.e119 (2022).
33. Collins, N. B. et al. PI3K activation allows immune evasion by promoting an inhibitory myeloid tumor microenvironment. *J. Immunother. Cancer* <https://doi.org/10.1136/jitc-2021-003402> (2022).
34. Mariathasan, S. et al. TGFβ attenuates tumour response to PD-L1 blockade by contributing to exclusion of T cells. *Nature* **554**, 544–548 (2018).
35. Kudo-Saito, C., Shirako, H., Takeuchi, T. & Kawakami, Y. Cancer metastasis is accelerated through immunosuppression during Snail-induced EMT of cancer cells. *Cancer Cell* **15**, 195–206 (2009).
36. Sume, S. S., Kantarci, A., Lee, A., Hasturk, H. & Trackman, P. C. Epithelial to mesenchymal transition in gingival overgrowth. *Am. J. Pathol.* **177**, 208–218 (2010).
37. Wang, K. et al. Knockdown of MMP-1 inhibits the progression of colorectal cancer by suppressing the PI3K/Akt/c-myc signaling pathway and EMT. *Oncol. Rep.* **43**, 1103–1112 (2020).
38. Konge, J. et al. Breast cancer stem cell-like cells generated during TGFβ-induced EMT are radioresistant. *Oncotarget* **9**, 23519–23531 (2018).
39. Kumagai, S. et al. The PD-1 expression balance between effector and regulatory T cells predicts the clinical efficacy of PD-1 blockade therapies. *Nat. Immunol.* **21**, 1346–1358 (2020).
40. Tu, S. et al. Overexpression of interleukin-1β induces gastric inflammation and cancer and mobilizes myeloid-derived suppressor cells in mice. *Cancer Cell* **14**, 408–419 (2008).
41. Nicolas, A. M. et al. Inflammatory fibroblasts mediate resistance to neoadjuvant therapy in rectal cancer. *Cancer Cell* **40**, 168–184.e113 (2022).
42. Yu, X. et al. The surface protein TIGIT suppresses T cell activation by promoting the generation of mature immunoregulatory dendritic cells. *Nat. Immunol.* **10**, 48–57 (2009).

43. Mair, F. et al. Extricating human tumour immune alterations from tissue inflammation. *Nature* **605**, 728–735 (2022).
44. Zhu, Y. et al. Toripalimab combined with definitive chemoradiotherapy in locally advanced oesophageal squamous cell carcinoma (EC-CRT-001): a single-arm, phase 2 trial. *Lancet Oncol.* **24**, 371–382 (2023).
45. Oweida, A. et al. Ionizing radiation sensitizes tumors to PD-L1 immune checkpoint blockade in orthotopic murine head and neck squamous cell carcinoma. *Oncoimmunology* **6**, e1356153 (2017).
46. Guan, H. et al. Safety and potential increased risk of toxicity of radiotherapy combined immunotherapy strategy. *Asia Pac. J. Clin. Oncol.* **19**, 35–50 (2023).
47. Gupta, A. et al. Radiotherapy promotes tumor-specific effector CD8<sup>+</sup> T cells via dendritic cell activation. *J. Immunol.* **189**, 558–566 (2012).
48. Kamada, T. et al. PD-1(+) regulatory T cells amplified by PD-1 blockade promote hyperprogression of cancer. *Proc. Natl Acad. Sci. USA* **116**, 9999–10008 (2019).
49. Itahashi, K. et al. BATF epigenetically and transcriptionally controls the activation program of regulatory T cells in human tumors. *Sci. Immunol.* **7**, eabk0957 (2022).
50. Solomon, I. et al. CD25-T(reg)-depleting antibodies preserving IL-2 signaling on effector T cells enhance effector activation and antitumor immunity. *Nat. Cancer* **1**, 1153–1166 (2020).
51. Kaplanov, I. et al. Blocking IL-1 $\beta$  reverses the immunosuppression in mouse breast cancer and synergizes with anti-PD-1 for tumor abrogation. *Proc. Natl Acad. Sci. USA* **116**, 1361–1369 (2019).
52. Qureshi, O. S. et al. Trans-endocytosis of CD80 and CD86: a molecular basis for the cell-extrinsic function of CTLA-4. *Science* **332**, 600–603 (2011).
53. Twyman-Saint Victor, C. et al. Radiation and dual checkpoint blockade activate non-redundant immune mechanisms in cancer. *Nature* **520**, 373–377 (2015).
54. Formenti, S. C. et al. Radiotherapy induces responses of lung cancer to CTLA-4 blockade. *Nat. Med.* **24**, 1845–1851 (2018).
55. Grapin, M. et al. Optimized fractionated radiotherapy with anti-PD-L1 and anti-TIGIT: a promising new combination. *J Immunother. Cancer* **7**, 160 (2019).
56. McShane, L. M. et al. REporting recommendations for tumor MARKer prognostic studies (REMARK). *Nat. Clin. Pract. Oncol.* **2**, 416–422 (2005).
57. Schulz, K. F., Altman, D. G., Moher, D. & CONSORT Group. CONSORT 2010 statement: updated guidelines for reporting parallel group randomised trials. *PLoS Med.* **7**, e1000251 (2010).
58. Sudo, N. et al. Clinical utility of ypTNM stage grouping in the 8th Edition of the American Joint Committee on Cancer TNM staging system for esophageal squamous cell carcinoma. *Ann. Surg. Oncol.* **28**, 650–660 (2021).
59. Bando, H. et al. TENERGY: multicenter phase II study of atezolizumab monotherapy following definitive Chemoradiotherapy with 5-FU plus cisplatin in patients with unresectable locally advanced esophageal squamous cell carcinoma. *BMC Cancer* **20**, 336 (2020).
60. Wu, T. et al. clusterProfiler 4.0: A universal enrichment tool for interpreting omics data. *Innovation* **2**, 100141 (2021).
61. Liberzon, A. et al. Molecular signatures database (MSigDB) 3.0. *Bioinformatics* **27**, 1739–1740 (2011).
62. Isella, C. et al. Stromal contribution to the colorectal cancer transcriptome. *Nat. Genet.* **47**, 312–319 (2015).
63. Hänzelmann, S., Castelo, R. & Guinney, J. GSVA: gene set variation analysis for microarray and RNA-seq data. *BMC Bioinform.* **14**, 7 (2013).
64. Dummer, R. et al. Combined PD-1, BRAF and MEK inhibition in advanced BRAF-mutant melanoma: safety run-in and biomarker cohorts of COMBI-i. *Nat. Med.* **26**, 1557–1563 (2020).
65. Kobayashi, T. et al. Isolation of tumor-infiltrating lymphocytes from preserved human tumor tissue specimens for downstream characterization. *STAR Protoc.* **3**, 101557 (2022).

## Acknowledgements

We express special thanks to all the participating patients and investigators. This investigator-initiated trial was supported by the Japan Agency for Medical Research and Development (grant no. 18ck0106420h0001). Chugai Pharmaceutical provided funds for the translational research and the study drugs. The funders had no role in the study design, data collection and analysis, decision to publish or preparation of the manuscript.

## Author contributions

All authors read and approved the manuscript. Study concepts: H.B., S. Kumagai, D.K., N.F. and T.K. Data acquisition: H.B., S. Kumagai, D.K., S.M., T.I., K.I., Y.T., T.H., S.F., M.K., T.T., H. Hara, S. Kadowaki, K.K., K.C., K.Y., S. Kageyama, H. Hojo, M.N., S. Koyama and T.K. Quality control of data and algorithms: H.B., S. Kumagai, H.T., M.F., N.F., H.M., H.N., K.S., T.Y. and T.K. Statistical analysis: H.B., S. Kumagai and M.W. Manuscript preparation: H.B., S. Kumagai, S. Koyama and T.K. Manuscript editing: All authors. Manuscript review: All authors.

## Competing interests

H.B. reports research funding from Ono Pharmaceutical and honoraria from Ono Pharmaceutical, Eli Lilly Japan and Taiho Pharmaceutical. S. Kumagai received honoraria from MSD and Chugai Pharmaceutical. S.M. received honoraria from Eli Lilly, Merck Biopharma and Chugai Pharmaceutical. K.I. received honoraria from MSD and Chugai Pharmaceutical. T.T. received honoraria from Ono Pharmaceutical, Bristol Myers Squibb, MSD and Taiho Pharmaceuticals. H. Hara reported honoraria from Asahi-Kasei, Bayer, Bristol Myers Squibb, Chugai, Daiichi Sankyo, Lilly, Merck Biopharma, MSD, Ono, Taiho, Takeda and Yakult; consulting or advisory roles from Bristol Myers Squibb, Boehringer Ingelheim, Daiichi Sankyo and Ono; and research grants from ALX Oncology, Amgen, Astellas, AstraZeneca, Bayer, BeiGene, Boehringer Ingelheim, Bristol Myers Squibb, Chugai, Daiichi Sankyo, Eisai, Janssen, MSD, Ono and Taiho. S. Kadowaki reports grants from Ono Pharmaceutical, Taiho Pharmaceutical, MSD, Nobel Pharmaceutical, Janssen Pharmaceutical, Bayer, Eli Lilly, Chugai Pharmaceutical and Daiichi Sankyo, and honoraria from Ono Pharmaceutical, Taiho Pharmaceutical, MSD, Daiichi Sankyo, Merck KgaA, Bristol Myers Squibb, Eli Lilly, Chugai Pharmaceutical, Bayer and Eisai. K.K. reports consulting fees from Ono Pharmaceutical, Bristol Myers Squibb, Beigene/Novartis, AstraZeneca, Roche, BAYER, Merck & Co., Merck Biopharma and Janssen; and honoraria from Ono Pharmaceutical and Bristol Myers Squibb. K.C. received grants from Bristol Myers Squibb and Ono for this study and honoraria from Bristol Myers Squibb, Chugai, Ono and Taiho outside of the submitted work. M.N. received personal fees from AstraZeneca, MSD, Varian Medical Systems and Illumina outside the submitted work. M.W. reports honoraria from Nihon Media Physics. S. Koyama reports receiving research funding from Otsuka Pharmaceutical and Chugai Pharmaceutical. H.M. received research funding from Ono Pharmaceutical, PFDeNA, Konica-Minolta, Ambry Genetics, Chugai, Guardant Health and Riken Genesis outside this study; and also serves as a board member of CureGene outside this study. H.N. received research funding and honoraria (lecture fees) from Ono Pharmaceutical, Bristol Myers Squibb, Chugai Pharmaceutical and MSD; honoraria (lecture fees) from Amgen; and research funding from Taiho Pharmaceutical, Daiichi Sankyo, Kyowa Kirin, Zenyaku Kogyo, Oncolys BioPharma, Debiopharma, Asahi-Kasei, Sysmex, Fujifilm, SRL, Astellas Pharmaceutical, Sumitomo Dainippon Pharma and BD Japan outside this study. He also serves as a board member and founder of Sustainable Cell Therapeutics and Cellian-Biclo outside

this study. K.S. reports receiving personal fees for advisory roles from Lilly, Bristol Myers Squibb, Takeda, Pfizer, Ono Pharmaceutical, Merck Pharmaceutical, Taiho Pharmaceutical, Astellas, Novartis, AbbVie, GSK, Daiichi Sankyo, Amgen, Boehringer Ingelheim, Guardant Health Japan and Janssen; receiving honoraria (lecture fees) from Takeda, Bristol Myers Squibb and Janssen; and receiving research funding from Astellas, Ono Pharmaceutical, Daiichi Sankyo, Taiho Pharmaceutical, Chugai, Merck Pharmaceutical, Medi Science, Eisai and Amgen, outside the submitted work. T.Y. reports research funding from Taiho, Ono, Chugai, Amgen, MSD, Daiichi Sankyo, Eisai, FALCO Biosystems, Genomedia, Molecular Health, Nippon Boehringer Ingelheim, Pfizer, Roche Diagnostics, Sysmex and Sanofi and honoraria from Bayer, Chugai, Merck Biopharma, MSD, Ono and Takeda. T.K. reports honoraria from Ono Pharmaceutical, Covidien Japan, MSD, Boehringer Ingelheim, Kyowa Kirin, EA Pharma, Bristol Myers Squibb, 3H Clinical Trial, AstraZeneca, Taiho Pharmaceutical, LiangYiHui Healthcare, Oncology News China, Japanese Society of Pharmaceutical Health Care and Sciences, Oncolys BioPharma and BMS; and research grants from Beigene Ltd., AstraZeneca, Chugai Pharmaceutical, Parexel International, Shionogi, Taiho Pharmaceutical, Astellas Amgen BioPharma, MSD and Ono Pharmaceutical. The other authors declare no competing interests.

## Additional information

**Extended data** is available for this paper at <https://doi.org/10.1038/s43018-025-00918-1>.

**Supplementary information** The online version contains supplementary material available at <https://doi.org/10.1038/s43018-025-00918-1>.

**Correspondence and requests for materials** should be addressed to Hideaki Bando or Takashi Kojima.


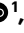
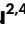




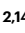



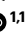

**Peer review information** *Nature Cancer* thanks Allison Furgal, Elizabeth Smyth and Wencheng Zhang for their contribution to the peer review of this work.

**Reprints and permissions information** is available at [www.nature.com/reprints](http://www.nature.com/reprints).

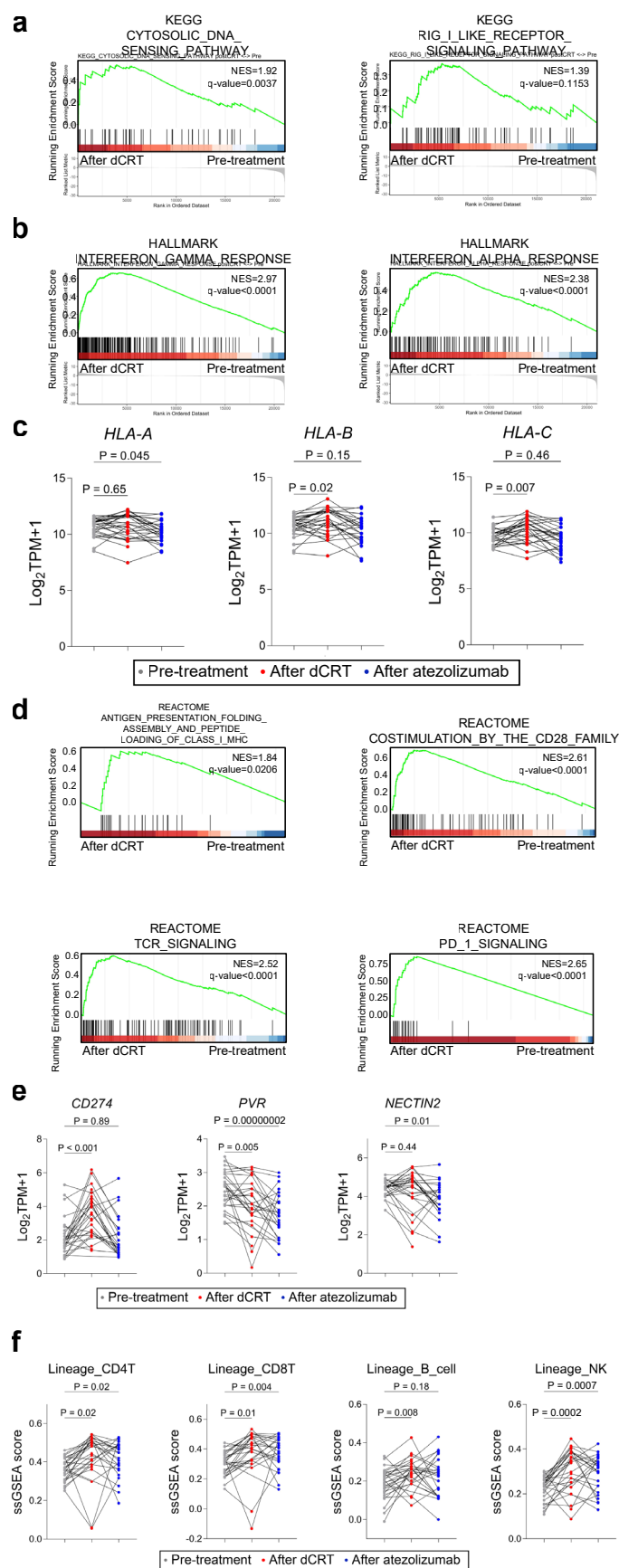
**Publisher's note** Springer Nature remains neutral with regard to jurisdictional claims in published maps and institutional affiliations.

**Open Access** This article is licensed under a Creative Commons Attribution-NonCommercial-NoDerivatives 4.0 International License, which permits any non-commercial use, sharing, distribution and reproduction in any medium or format, as long as you give appropriate credit to the original author(s) and the source, provide a link to the Creative Commons licence, and indicate if you modified the licensed material. You do not have permission under this licence to share adapted material derived from this article or parts of it. The images or other third party material in this article are included in the article's Creative Commons licence, unless indicated otherwise in a credit line to the material. If material is not included in the article's Creative Commons licence and your intended use is not permitted by statutory regulation or exceeds the permitted use, you will need to obtain permission directly from the copyright holder. To view a copy of this licence, visit <http://creativecommons.org/licenses/by-nc-nd/4.0/>.

© The Author(s) 2025

Hideaki Bando <sup>1,16</sup>✉, Shogo Kumagai<sup>2,3,16</sup>, Daisuke Kotani <sup>1</sup>, Saori Mishima<sup>1</sup>, Takuma Irie<sup>2</sup>, Kota Itahashi<sup>2</sup>, Yosuke Tanaka <sup>3</sup>, Takumi Habu<sup>2,4</sup>, Sayuri Fukaya<sup>2,5</sup>, Masaki Kondo<sup>2,6</sup>, Takahiro Tsushima<sup>7</sup>, Hiroki Hara<sup>8</sup>, Shigenori Kadowaki <sup>9</sup>, Ken Kato <sup>10</sup>, Keisho Chin<sup>11</sup>, Kensei Yamaguchi<sup>11</sup>, Shun-ichiro Kageyama <sup>12</sup>, Hidehiro Hojo<sup>12</sup>, Masaki Nakamura <sup>12</sup>, Hidenobu Tachibana<sup>12</sup>, Masashi Wakabayashi<sup>13</sup>, Makoto Fukui<sup>13</sup>, Nozomu Fuse<sup>13</sup>, Shohei Koyama <sup>2,14</sup>, Hiroyuki Mano <sup>3</sup>, Hiroyoshi Nishikawa <sup>2</sup>, Kohei Shitara <sup>1</sup>, Takayuki Yoshino <sup>1,15</sup> & Takashi Kojima <sup>1</sup>✉

<sup>1</sup>Department of Gastroenterology and Gastrointestinal Oncology, National Cancer Center Hospital East, Kashiwa, Japan. <sup>2</sup>Division of Cancer Immunology, Research Institute/Exploratory Oncology Research and Clinical Trial Center, National Cancer Center, Tokyo/Kashiwa, Japan. <sup>3</sup>Division of Cellular Signaling, Research Institute, National Cancer Center, Tokyo, Japan. <sup>4</sup>Department of Gastric Surgery, National Cancer Center Hospital East, Kashiwa, Japan. <sup>5</sup>Department of Obstetrics and Gynecology, Graduate School of Medicine, The University of Tokyo, Tokyo, Japan. <sup>6</sup>Department of Neurosurgery, Nagoya University Graduate School of Medicine, Nagoya, Japan. <sup>7</sup>Division of Gastrointestinal Oncology Shizuoka Cancer Center, Shizuoka, Japan. <sup>8</sup>Department of Gastroenterology, Saitama Cancer Center, Saitama, Japan. <sup>9</sup>Department of Clinical Oncology, Aichi Cancer Center Hospital, Nagoya, Japan. <sup>10</sup>Department of Gastrointestinal Medical Oncology, National Cancer Center Hospital, Tokyo, Japan. <sup>11</sup>Department of Gastroenterological Chemotherapy, Cancer Institute Hospital of Japanese Foundation for Cancer Research, Tokyo, Japan. <sup>12</sup>Division of Radiation Oncology and Particle Therapy, National Cancer Center Hospital East, Kashiwa, Japan. <sup>13</sup>Clinical Research Support Office, National Cancer Center Hospital East, Kashiwa, Japan. <sup>14</sup>Department of Respiratory Medicine and Clinical Immunology, Osaka University Graduate School of Medicine, Osaka, Japan. <sup>15</sup>Kindai University Faculty of Medicine, Osaka, Japan. <sup>16</sup>These authors contributed equally: Hideaki Bando, Shogo Kumagai. ✉e-mail: [hbando@east.ncc.go.jp](mailto:hbando@east.ncc.go.jp); [takojima@east.ncc.go.jp](mailto:takojima@east.ncc.go.jp)

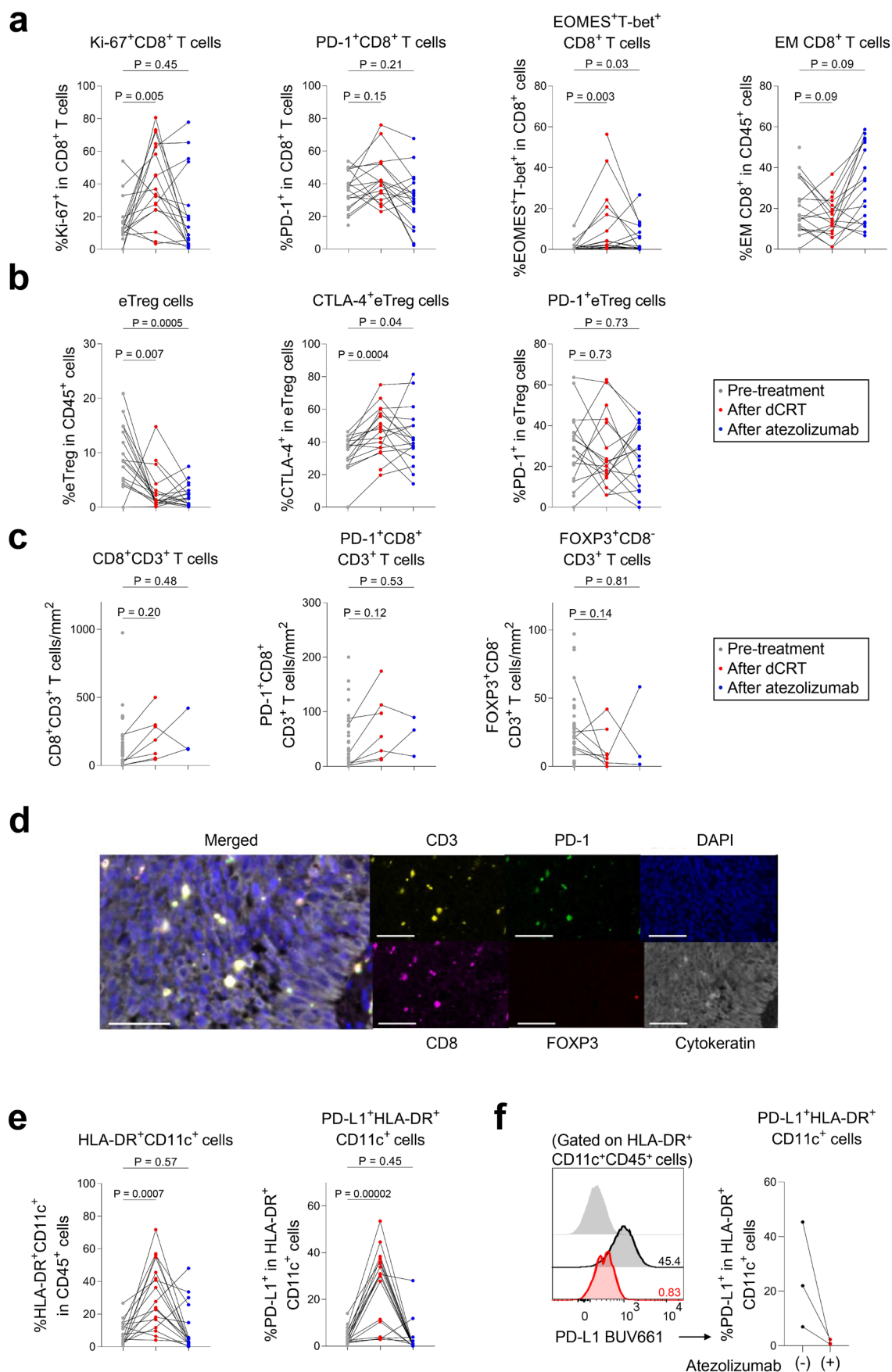


Extended Data Fig. 1 | See next page for caption.



**Extended Data Fig. 1 | Transcriptomic analysis of antitumor immune responses caused by combination therapy with dCRT and atezolizumab.** Gene expression in ESCCs after dCRT was compared with that in ESCCs prior to dCRT by performing GSEA with the indicated gene sets. **(a)** Enrichment plots of the indicated gene sets (left, KEGG CYTOSOLIC DNA SENSING PATHWAY; right, KEGG RIG-I LIKE RECEPTOR SIGNALING PATHWAY) are shown. **(b)** Enrichment plots of the indicated gene sets (left, HALLMARK INTERFERON GAMMA RESPONSE; right, HALLMARK INTERFERON ALPHA RESPONSE) are shown. **(c)** Gene expression of *HLA-A*, *HLA-B* and *HLA-C* in ESCCs during treatment (pretreatment (N = 28 patients), after dCRT (N = 25 patients) and after atezolizumab treatment (N = 25 patients)) was evaluated. Summaries of the TPM values of the indicated genes are shown. **(d)** Enrichment plots of the indicated gene sets (left upper, REACTOME ANTIGEN PRESENTATION FOLDING ASSEMBLY AND PEPTIDE LOADING OF CLASS I MHC; right upper, REACTOME COSTIMULATION BY THE CD28 FAMILY; left lower, REACTOME TCR SIGNALING; right lower, REACTOME PD-1 SIGNALING) are shown. **(e)** Gene expression of the immune checkpoint molecules *CD274*,

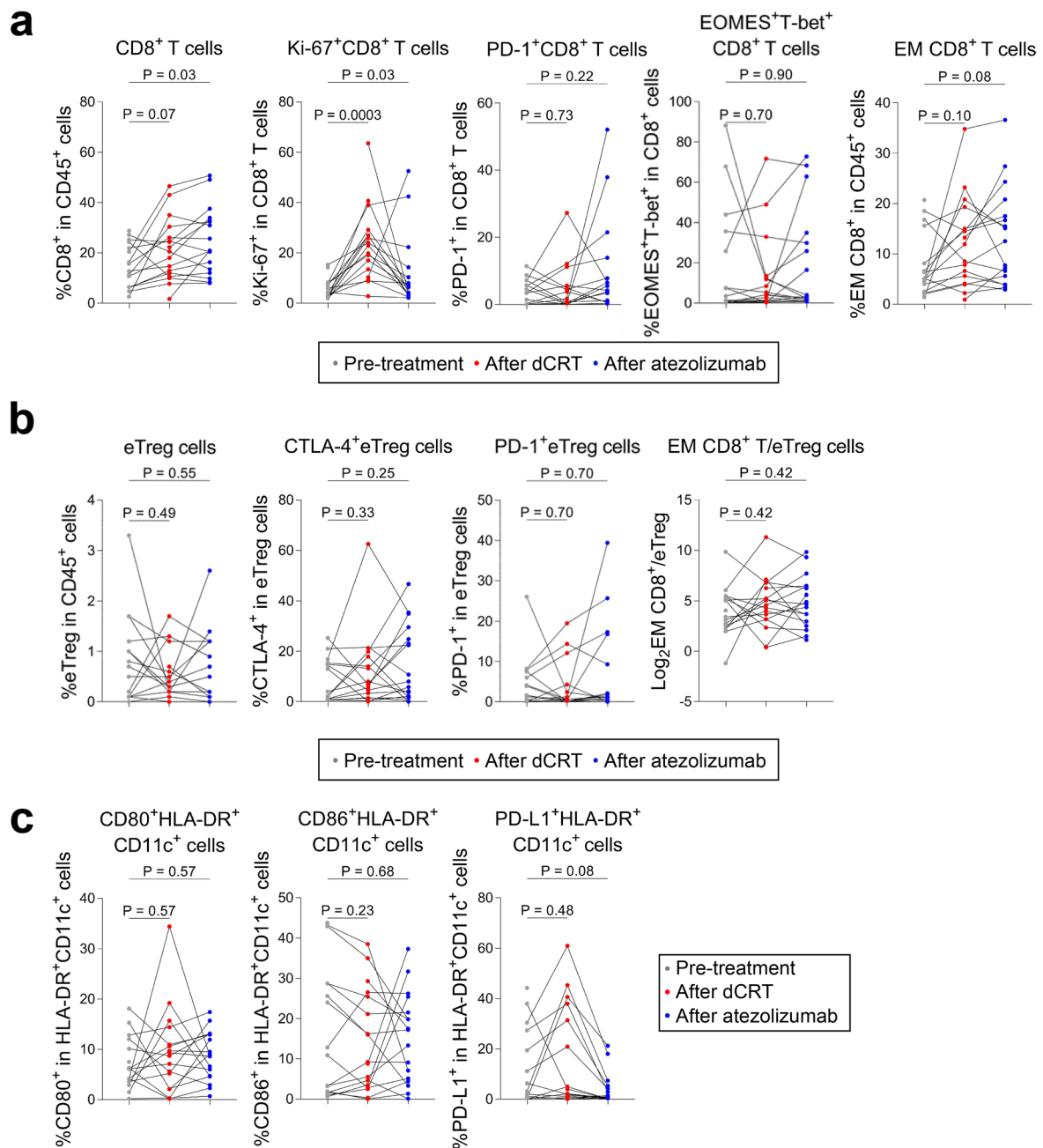
*PVR* and *NECTIN2* in ESCCs during treatment (pretreatment (N = 28 patients), after dCRT (N = 25 patients) and after atezolizumab treatment (N = 25 patients)) was evaluated. Summaries of the TPM values of the indicated genes are shown. **(f)** ssGSEA scores from the indicated gene sets were calculated from gene expression in ESCCs during treatment (pretreatment (N = 28 patients), after dCRT (N = 25 patients) and after atezolizumab treatment (N = 25 patients)). Summaries of ssGSEA scores from the indicated gene sets are shown. **(c,e,f)** Gray, pretreatment; red, after dCRT; blue, after atezolizumab. P values were calculated by one-way ANOVA. For multiple comparisons, Holm–Sidak’s test was performed. The differences with  $P \leq 0.05$  were considered significant. Significant differences were found between the pretreatment, after dCRT, and after atezolizumab stages in *HLA-A* ( $P = 0.045$ ), *PVR* ( $P = 0.00000002$ ), *NECTIN2* ( $P = 0.01$ ), lineage CD4T ( $P = 0.02$ ), lineage CD8T ( $P = 0.004$ ), and lineage NK ( $P = 0.0007$ ); however, no differences were found in *HLA-B* ( $P = 0.15$ ), *HLA-C* ( $P = 0.46$ ), *CD274* ( $P = 0.89$ ), and lineage B cell ( $P = 0.18$ ).



Extended Data Fig. 2 | See next page for caption.

**Extended Data Fig. 2 | Immunological analysis of TILs affected by combination therapy with dCRT and atezolizumab. (a, b and e)** TILs extracted from ESCCs during treatment (pretreatment (N = 18 patients), after dCRT (N = 18 patients) and after atezolizumab treatment (N = 18 patients)) were subjected to FCM. **(a)** Summary of Ki-67<sup>+</sup> CD8<sup>+</sup> T, PD-1<sup>+</sup> CD8<sup>+</sup> T, EOMES<sup>+</sup> T-bet<sup>+</sup> CD8<sup>+</sup> T, and EM CD8<sup>+</sup> T cells in the TME during treatment (pretreatment, post-dCRT, and post-atezolizumab treatment). **(b)** Summaries of FOXP3<sup>high</sup> CD45RA<sup>+</sup> CD4<sup>+</sup> CD3<sup>+</sup> T cells, CTLA-4<sup>+</sup> FOXP3<sup>high</sup> CD45RA<sup>+</sup> CD4<sup>+</sup> CD3<sup>+</sup> T cells, PD-1<sup>+</sup> FOXP3<sup>high</sup> CD45RA<sup>+</sup> CD4<sup>+</sup> CD3<sup>+</sup> T cells in the TME during treatment (pretreatment, post-dCRT, and post-atezolizumab treatment) are shown. **(c and d)** Multiplex IHC of ESCCs during treatment (pretreatment (N = 40 patients), after dCRT (N = 7 patients) and after atezolizumab treatment (N = 3 patients)) was performed. **(c)** Summaries of intratumor CD8<sup>+</sup> CD3<sup>+</sup> T cells (left), PD-1<sup>+</sup> CD8<sup>+</sup> CD3<sup>+</sup> T cells (middle) and FOXP3<sup>+</sup> CD8<sup>+</sup> CD3<sup>+</sup> T cells (right) are shown. **(d)** Representative pictures of multiplexed IHC of ESCC samples for the indicated markers (CD3, yellow; PD-1, green; DAPI, blue; CD8, purple; FOXP3, red; cytokeratin, white) are shown (N = 1 patient). Scale bar: 50  $\mu$ m. **(e)** Summaries of HLA-DR<sup>+</sup> CD11c<sup>+</sup> CD45<sup>+</sup> cells and

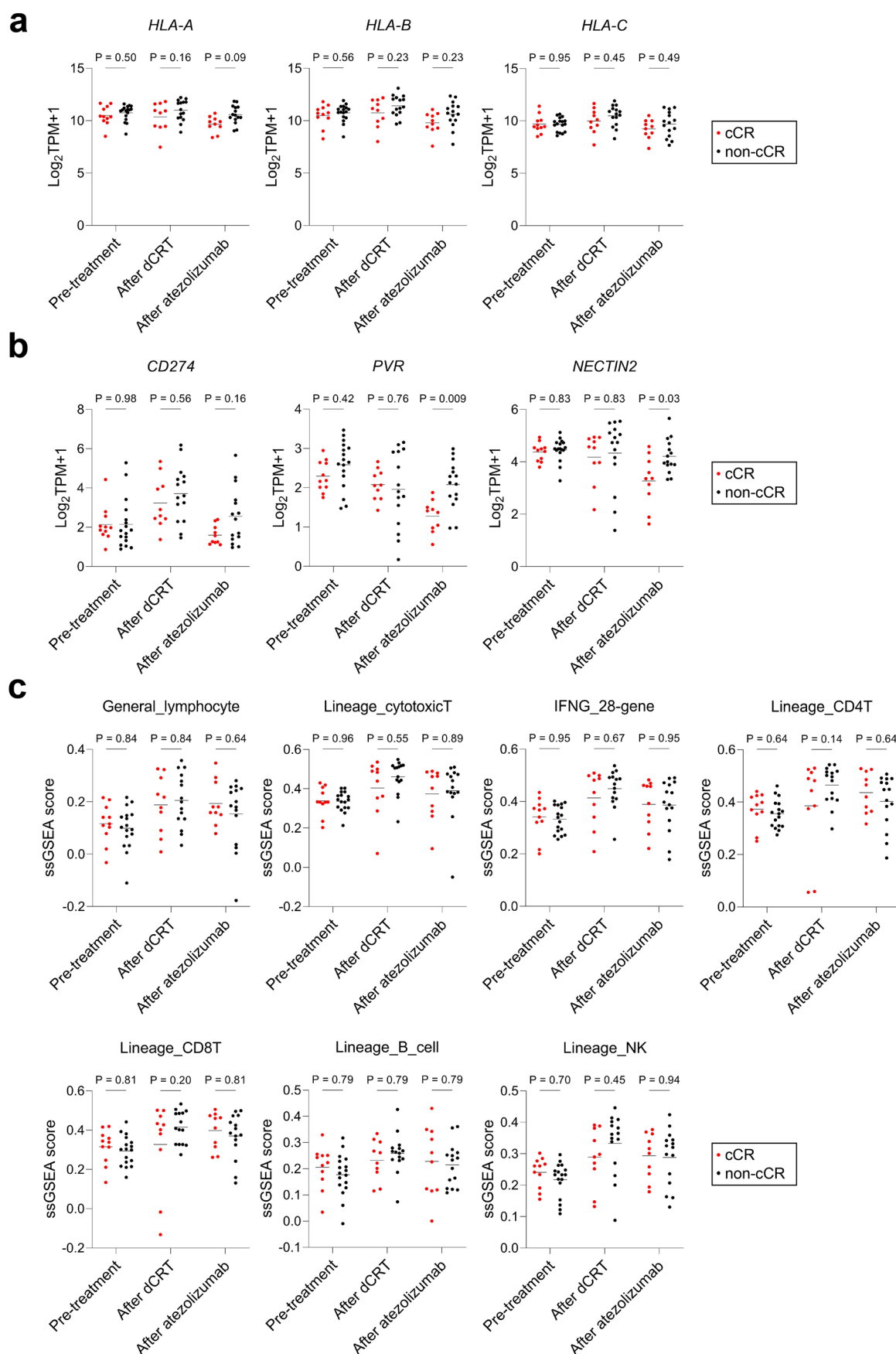
PD-L1<sup>+</sup> HLA-DR<sup>+</sup> CD11c<sup>+</sup> CD45<sup>+</sup> cells in the TME during treatment (pretreatment, after dCRT and after atezolizumab treatment) are shown. **(f)** PBMCs isolated from three patients with ESCC were incubated with or without atezolizumab for 20 min at 37°C. After incubation, these PBMC samples were stained with antibodies for FCM analysis. Representative histograms (left) and summaries (right) of PD-L1 expression of HLA-DR<sup>+</sup> CD11c<sup>+</sup> CD45<sup>+</sup> cells from PBMCs incubated without atezolizumab (black) or with atezolizumab (red) are shown. **(a, b, c and e)** Gray, pretreatment; red, after dCRT; blue, after atezolizumab. P values were calculated by one-way ANOVA. For multiple comparisons, Holm–Sidak’s test was performed. Significant differences were found between the pretreatment, after dCRT, and after atezolizumab stages in EOMES<sup>+</sup> T-bet<sup>+</sup> CD8<sup>+</sup> T cells (P = 0.03), eTreg cells (P = 0.0005), and CTLA-4<sup>+</sup> eTreg cells (P = 0.04), but not Ki-67<sup>+</sup> CD8<sup>+</sup> T (P = 0.45), PD-1<sup>+</sup> CD8<sup>+</sup> T (P = 0.21), EM CD8<sup>+</sup> T cells (P = 0.09), PD-1<sup>+</sup> eTreg cells (P = 0.73), CD8<sup>+</sup> CD3<sup>+</sup> T cells (P = 0.48), PD-1<sup>+</sup> CD8<sup>+</sup> CD3<sup>+</sup> T cells (P = 0.53) and FOXP3<sup>+</sup> CD8<sup>+</sup> CD3<sup>+</sup> T cells (P = 0.81), HLA-DR<sup>+</sup> CD11c<sup>+</sup> CD45<sup>+</sup> cells (P = 0.57), nor PD-L1<sup>+</sup> HLA-DR<sup>+</sup> CD11c<sup>+</sup> CD45<sup>+</sup> cells (P = 0.45).



**Extended Data Fig. 3 | Immunological analysis of PBMCs affected by combination therapy with dCRT and atezolizumab. (a-c)** PBMCs during treatment (pretreatment (N = 16 patients), after dCRT (N = 17 patients) and after atezolizumab treatment (N = 17 patients)) were subjected to FCM. **(a)** Summaries of CD8<sup>+</sup> T cells, Ki-67<sup>+</sup> CD8<sup>+</sup> T cells, PD-1<sup>+</sup>CD8<sup>+</sup> T cells, EOMES<sup>+</sup>T-bet<sup>+</sup>CD8<sup>+</sup> T cells and CCR7<sup>+</sup>CD45RA<sup>+</sup> (EM) CD8<sup>+</sup> T cells during treatment are shown. **(b)** Summaries of FOXP3<sup>high</sup>CD45RA<sup>+</sup>CD4<sup>+</sup>CD3<sup>+</sup> T cells, CTLA-4<sup>+</sup>FOXP3<sup>high</sup>CD45RA<sup>+</sup>CD4<sup>+</sup>CD3<sup>+</sup> T cells, PD-1<sup>+</sup>FOXP3<sup>high</sup>CD45RA<sup>+</sup>CD4<sup>+</sup>CD3<sup>+</sup> T cells and the ratio of CCR7<sup>+</sup>CD45RA<sup>+</sup> (EM)CD8<sup>+</sup> T cells to FOXP3<sup>high</sup>CD45RA<sup>+</sup>CD4<sup>+</sup>CD3<sup>+</sup> T cells during treatment are shown. **(c)** Summaries of CD80<sup>+</sup>HLA-DR<sup>+</sup>CD11c<sup>+</sup>CD45<sup>+</sup> cells, CD86<sup>+</sup>HLA-DR<sup>+</sup>CD11c<sup>+</sup>CD45<sup>+</sup> cells and PD-L1<sup>+</sup>HLA-DR<sup>+</sup>CD11c<sup>+</sup>CD45<sup>+</sup> cells during treatment

(pretreatment, after dCRT and after atezolizumab treatment) are shown. **(a-c)** Gray, pretreatment; red, after dCRT; blue, after atezolizumab. P values were calculated by one-way ANOVA. For multiple comparisons, Holm-Sidak's test was performed. Significant differences were found between the pretreatment, after dCRT, and after atezolizumab stages in CD8<sup>+</sup> T cells (P = 0.03) and Ki-67<sup>+</sup> CD8<sup>+</sup> T cells (P = 0.03), but not PD-1<sup>+</sup>CD8<sup>+</sup> T cells (P = 0.22), EOMES<sup>+</sup>T-bet<sup>+</sup>CD8<sup>+</sup> T cells (P = 0.90), EM CD8<sup>+</sup> T cells (P = 0.08), eTreg cells (P = 0.55), CTLA-4<sup>+</sup> eTreg cells (P = 0.25), PD-1<sup>+</sup> eTreg cells (P = 0.70), or the ratio of EM CD8<sup>+</sup> T cells to eTreg cells (P = 0.42), CD80<sup>+</sup>HLA-DR<sup>+</sup>CD11c<sup>+</sup>CD45<sup>+</sup> cells (P = 0.57), CD86<sup>+</sup>HLA-DR<sup>+</sup>CD11c<sup>+</sup>CD45<sup>+</sup> cells (P = 0.68), nor PD-L1<sup>+</sup>HLA-DR<sup>+</sup>CD11c<sup>+</sup>CD45<sup>+</sup> cells (P = 0.08).

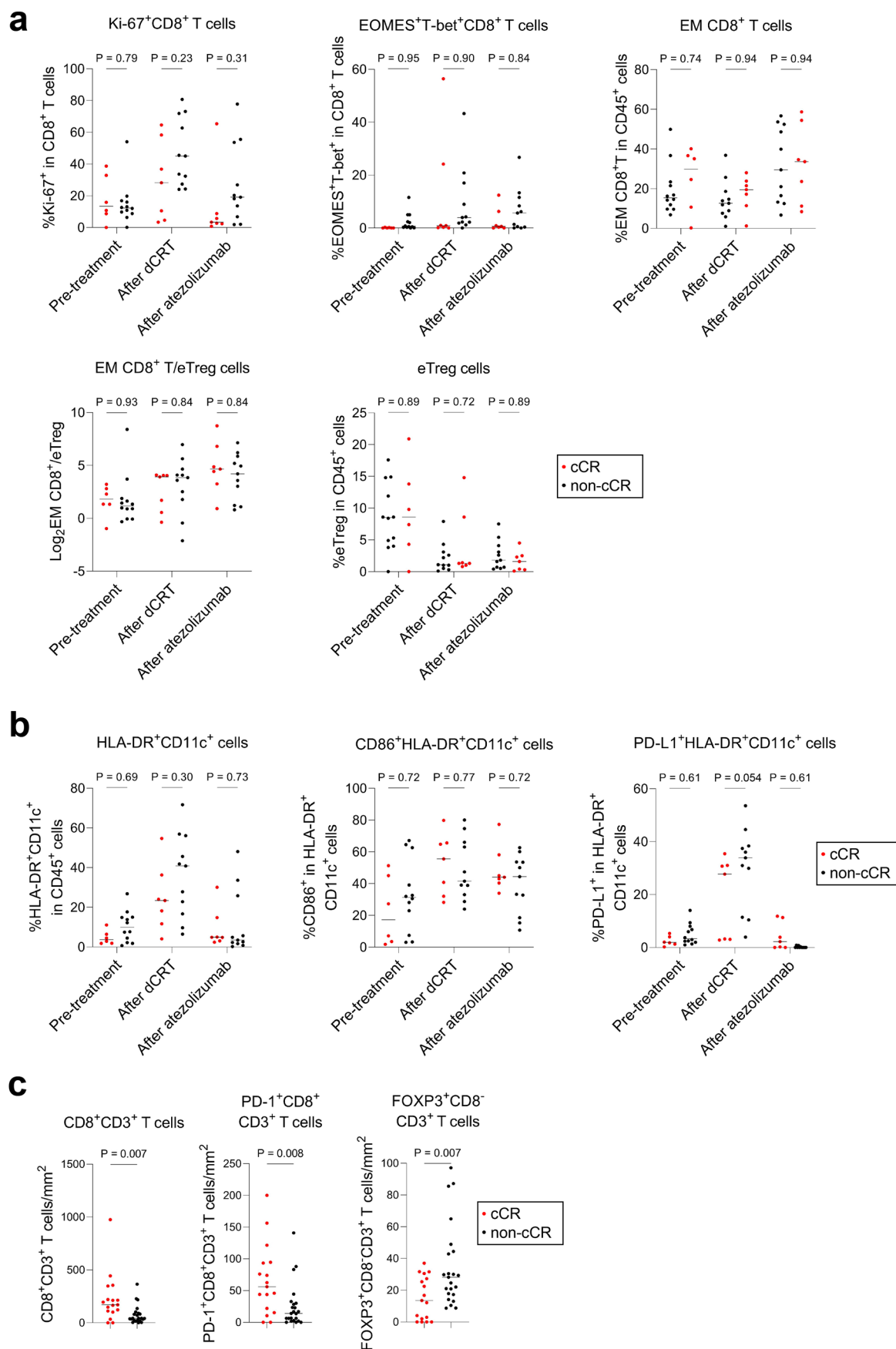




Extended Data Fig. 4 | See next page for caption.

**Extended Data Fig. 4 | Transcriptomic analysis of ESCCs during combination therapy with dCRT and atezolizumab.** (a) Gene expression of *HLA-A*, *HLA-B* and *HLA-C* in ESCCs during treatment (pretreatment (cCR, N = 11 patients; non-cCR, N = 17 patients), after dCRT (cCR, N = 10 patients; non-cCR, N = 15 patients) and after atezolizumab treatment (cCR, N = 10 patients; non-cCR, N = 15 patients)) was evaluated according to treatment response. Summaries of the TPM values of the indicated genes are shown. (b) Gene expression of *CD274*, *PVR* and *NECTIN2* in ESCCs during treatment (pretreatment (cCR, N = 11 patients; non-cCR, N = 17 patients), after dCRT (cCR, N = 10 patients; non-cCR, N = 15 patients) and after atezolizumab treatment (cCR, N = 10 patients; non-cCR, N = 15 patients)) was evaluated according to treatment response. Summaries of the TPM values of the indicated genes are shown. (c) ssGSEA scores from the indicated gene sets were calculated from gene expression in ESCCs during treatment (pretreatment (cCR, N = 11 patients; non-cCR, N = 17 patients), after dCRT (cCR, N = 10 patients; non-cCR, N = 15 patients) and after atezolizumab treatment (cCR, N = 10 patients; non-cCR, N = 15 patients)) according to treatment response. (a–c) Gray, unstained control; red, patients who achieved cCR (cCR cases); black, patients who did not achieve cCR (non-cCR cases). Bars, mean; P values were calculated by two-way

ANOVA. For multiple comparisons, Holm–Sidak’s test was performed. Significant differences in *PVR* ( $P = 0.009$ ) and in *NECTIN2* ( $P = 0.03$ ) were found between the cCR and non-cCR cases following atezolizumab treatment, but no significant differences were found pretreatment (*PVR*  $P = 0.42$ ; *NECTIN2*  $P = 0.83$ ) or after dCRT (*PVR*  $P = 0.76$ ; *NECTIN2*  $P = 0.83$ ). Furthermore, there were no significant differences between the cCR and non-cCR cases at any time point for *HLA-A* (pretreatment  $P = 0.50$ ; after dCRT  $P = 0.16$ ; after atezolizumab  $P = 0.09$ ), *HLA-B* (pretreatment  $P = 0.56$ ; after dCRT  $P = 0.23$ ; after atezolizumab  $P = 0.23$ ), *HLA-C* (pretreatment  $P = 0.95$ ; after dCRT  $P = 0.45$ ; after atezolizumab  $P = 0.49$ ), *CD274* (pretreatment  $P = 0.98$ ; after dCRT  $P = 0.56$ ; after atezolizumab  $P = 0.16$ ), general lymphocyte (pretreatment  $P = 0.84$ ; after dCRT  $P = 0.84$ ; after atezolizumab  $P = 0.64$ ), lineage cytotoxic T (pretreatment  $P = 0.96$ ; after dCRT  $P = 0.55$ ; after atezolizumab  $P = 0.89$ ), IFNG28 gene (pretreatment  $P = 0.95$ ; after dCRT  $P = 0.67$ ; after atezolizumab  $P = 0.95$ ), lineage CD4T (pretreatment  $P = 0.64$ ; after dCRT  $P = 0.14$ ; after atezolizumab  $P = 0.64$ ), lineage CD8T (pretreatment  $P = 0.81$ ; after dCRT  $P = 0.20$ ; after atezolizumab  $P = 0.81$ ), lineage B cell (pretreatment, after dCRT, and after atezolizumab, all  $P = 0.79$ ), nor lineage NK (pretreatment  $P = 0.70$ ; after dCRT  $P = 0.45$ ; after atezolizumab  $P = 0.94$ ).

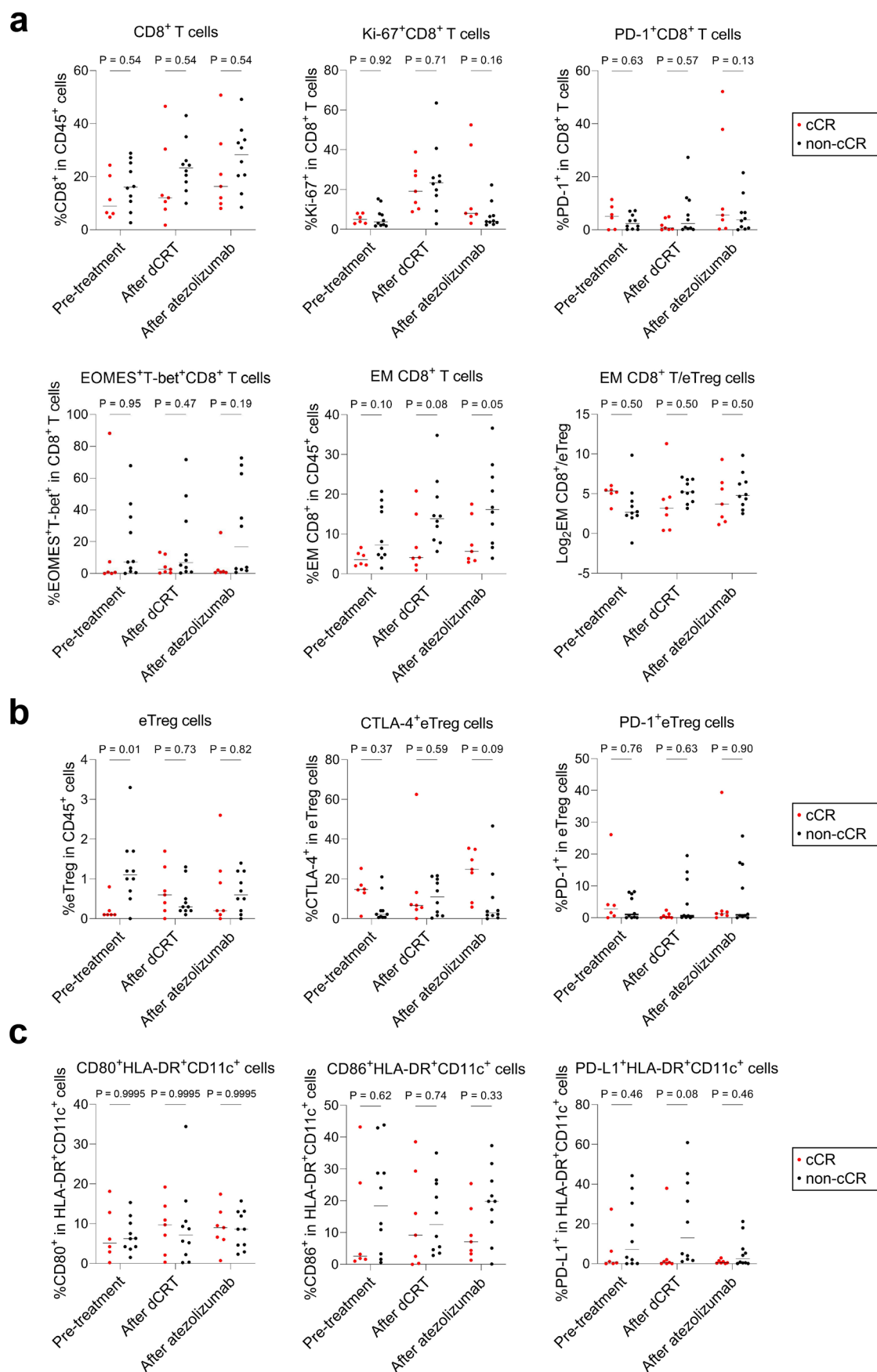


Extended Data Fig. 5 | See next page for caption.

**Extended Data Fig. 5 | Additional analysis of TILs during combination therapy with dCRT and atezolizumab. (a and b)** TILs extracted from ESCCs during treatment (pretreatment (cCR, N = 6 patients; non-cCR, N = 12 patients), post-dCRT (cCR, N = 7 patients; non-cCR, N = 11 patients), and post-atezolizumab treatment (cCR, N = 7 patients; non-cCR, N = 11 patients) were subjected to FCM. **(a)** Summaries of Ki-67<sup>+</sup>CD8<sup>+</sup> T cells (upper left), EOMES<sup>+</sup>T-bet<sup>+</sup>CD8<sup>+</sup> T cells (upper middle), CCR7 CD45RA<sup>+</sup> (EM) CD8<sup>+</sup> T cells (upper right), and the ratio of CCR7 CD45RA<sup>+</sup> (EM) CD8<sup>+</sup> T cells to FOXP3<sup>high</sup>CD45RA<sup>+</sup>CD4<sup>+</sup>CD3<sup>+</sup> T (lower left) and FOXP3<sup>high</sup>CD45RA<sup>+</sup>CD4<sup>+</sup>CD3<sup>+</sup> T cells (lower right) during treatment are shown according to treatment response. **(b)** Summaries of HLA-DR<sup>+</sup>CD11c<sup>+</sup>CD45<sup>+</sup> cells (left), CD86<sup>+</sup>HLA-DR<sup>+</sup>CD11c<sup>+</sup>CD45<sup>+</sup> cells (middle) and PD-L1<sup>+</sup>HLA-DR<sup>+</sup>CD11c<sup>+</sup>CD45<sup>+</sup> cells (right) during treatment (pretreatment, after dCRT and after atezolizumab treatment) are shown according to treatment response. Red, patients who achieved cCR (cCR cases); black, patients who did not achieve cCR (non-cCR cases). Bars, mean; P values were calculated by two-way ANOVA. For multiple comparisons, Holm–Sidak’s test was performed. **(c)** Multiplex IHC of pretreatment ESCC samples was performed. Summaries of intratumor CD8<sup>+</sup>CD3<sup>+</sup> T cells (left), PD-1<sup>+</sup>CD8<sup>+</sup>CD3<sup>+</sup> T cells (middle) and FOXP3<sup>+</sup>CD8<sup>+</sup>CD3<sup>+</sup> T

cells (right) are shown according to treatment response (cCR (N = 17 patients) and non-cCR (N = 23 patients)). Red, cCR cases; black, non-cCR cases. Bars, mean; P values were calculated by unpaired two-tailed t-test. Between the cCR and non-cCR cases, significant differences were found in intratumor CD8<sup>+</sup>CD3<sup>+</sup> T cells (P = 0.007), PD-1<sup>+</sup>CD8<sup>+</sup>CD3<sup>+</sup> T cells (P = 0.008) and FOXP3<sup>+</sup>CD8<sup>+</sup>CD3<sup>+</sup> T cells (P = 0.007). Comparing the cCR and non-cCR cases pretreatment, after dCRT, and after atezolizumab, revealed no significant differences at any time point for Ki-67<sup>+</sup>CD8<sup>+</sup> T cells (pretreatment P = 0.79; after dCRT P = 0.23; after atezolizumab P = 0.31), EOMES<sup>+</sup>T-bet<sup>+</sup>CD8<sup>+</sup> T cells (pretreatment P = 0.95; after dCRT P = 0.90; after atezolizumab P = 0.84), EM CD8<sup>+</sup> T cells (pretreatment P = 0.74; after dCRT P = 0.94; after atezolizumab P = 0.94), the ratio of EM CD8<sup>+</sup> T cells to eTreg cells (pretreatment P = 0.93; after dCRT P = 0.84; after atezolizumab P = 0.84), and eTreg cells (pretreatment P = 0.89; after dCRT P = 0.72; after atezolizumab P = 0.89), HLA-DR<sup>+</sup>CD11c<sup>+</sup>CD45<sup>+</sup> cells (pretreatment P = 0.69; after dCRT P = 0.30; after atezolizumab P = 0.73), CD86<sup>+</sup>HLA-DR<sup>+</sup>CD11c<sup>+</sup> cells (pretreatment P = 0.72; after dCRT P = 0.77; after atezolizumab P = 0.72), nor PD-L1<sup>+</sup>HLA-DR<sup>+</sup>CD11c<sup>+</sup> cells (pretreatment P = 0.61; after dCRT P = 0.054; after atezolizumab P = 0.61).

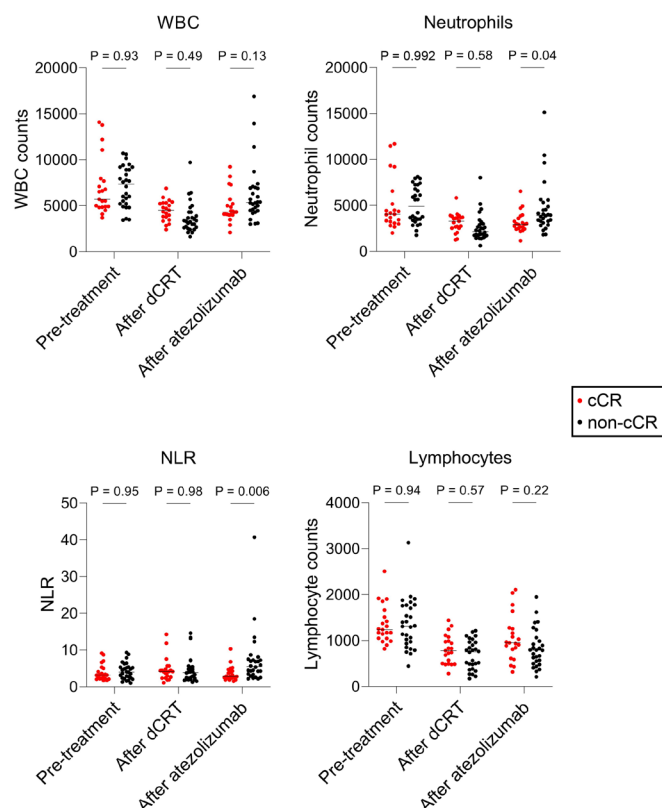




Extended Data Fig. 6 | See next page for caption.

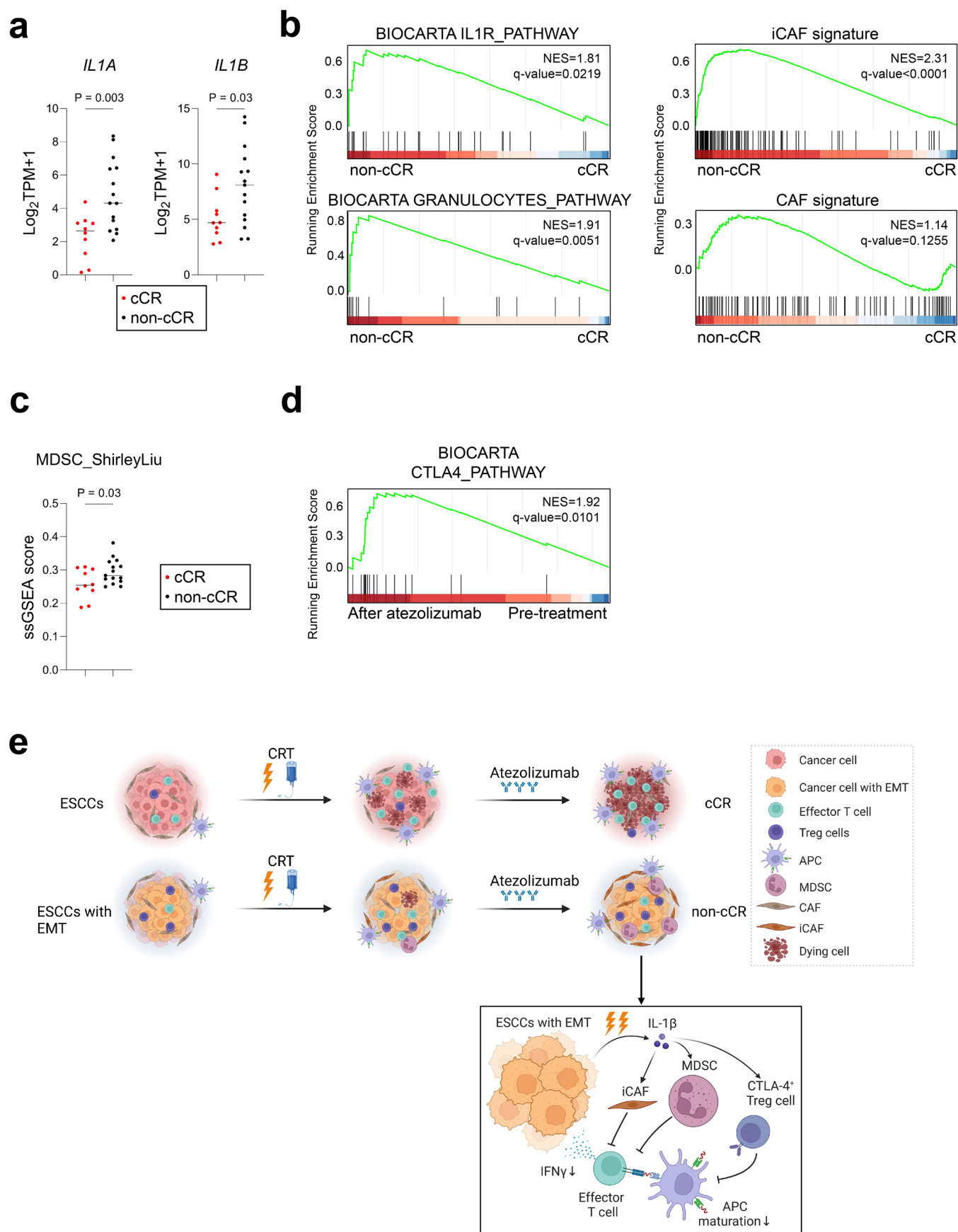
**Extended Data Fig. 6 | Immunological analysis of PBMCs during combination therapy with dCRT and atezolizumab. (a–c)** PBMCs during treatment (pretreatment (cCR, N = 6 patients; non-cCR, N = 10 patients), post-dCRT (cCR, N = 7 patients; non-cCR, N = 10 patients), and post-atezolizumab treatment (cCR, N = 7 patients; non-cCR, N = 10 patients)) were subjected to FCM. **(a)** Summaries of CD8<sup>+</sup> T cells (upper left), Ki-67<sup>+</sup> CD8<sup>+</sup> T cells (upper middle), PD-1<sup>+</sup> CD8<sup>+</sup> T cells (upper right), EOMES<sup>+</sup> T-bet<sup>+</sup> CD8<sup>+</sup> T cells (lower left), CCR7 CD45RA<sup>+</sup> (EM) CD8<sup>+</sup> T cells (lower middle), and the ratio of CCR7 CD45RA<sup>+</sup> (EM) CD8<sup>+</sup> T cells to FOXP3<sup>high</sup> CD45RA<sup>+</sup> CD4<sup>+</sup> CD3<sup>+</sup> T cells (lower right) during treatment are shown according to treatment response. **(b)** Summary of FOXP3<sup>high</sup> CD45RA<sup>+</sup> CD4<sup>+</sup> CD3<sup>+</sup> T, CTLA-4<sup>+</sup> FOXP3<sup>high</sup> CD45RA<sup>+</sup> CD4<sup>+</sup> CD3<sup>+</sup> T, and PD-1<sup>+</sup> FOXP3<sup>high</sup> CD45RA<sup>+</sup> CD4<sup>+</sup> CD3<sup>+</sup> T cells during treatment according to treatment response. **(c)** Summaries of CD80<sup>+</sup> HLA-DR<sup>+</sup> CD11c<sup>+</sup> CD45<sup>+</sup> cells, CD86<sup>+</sup> HLA-DR<sup>+</sup> CD11c<sup>+</sup> CD45<sup>+</sup> cells and PD-L1<sup>+</sup> HLA-DR<sup>+</sup> CD11c<sup>+</sup> CD45<sup>+</sup> cells during treatment (pretreatment, after dCRT and after atezolizumab treatment) are shown according to treatment response. **(a–c)** Red, patients who achieved cCR (cCR cases); black, patients who did not achieve cCR (non-cCR cases). Bars, mean; P values were calculated by two-way ANOVA. For multiple comparisons, Holm–Sidak's test was performed. Between

the cCR and non-cCR cases significant differences were found in eTreg cells (P = 0.01) pretreatment, but there were no significant differences after dCRT (P = 0.73) or after atezolizumab (P = 0.82). Further, there were no significant differences between the cCR and non-cCR cases at any time point for CD8<sup>+</sup> T cells (pretreatment, after dCRT, and after atezolizumab, all Ps = 0.54), Ki-67<sup>+</sup> CD8<sup>+</sup> T cells (pretreatment P = 0.92; after dCRT P = 0.71; after atezolizumab P = 0.16), PD-1<sup>+</sup> CD8<sup>+</sup> T cells (pretreatment P = 0.63; after dCRT P = 0.57; after atezolizumab P = 0.13), EOMES<sup>+</sup> T-bet<sup>+</sup> CD8<sup>+</sup> T cells (pretreatment P = 0.95; after dCRT P = 0.47; after atezolizumab P = 0.19), EM CD8<sup>+</sup> T cells (pretreatment P = 0.10; after dCRT P = 0.08; after atezolizumab P = 0.05), and the ratio of EM CD8<sup>+</sup> T cells to eTreg cells (pretreatment, after dCRT, and after atezolizumab, all Ps = 0.50), CTLA-4<sup>+</sup> eTreg cells (pretreatment P = 0.37; after dCRT P = 0.59; after atezolizumab P = 0.09), PD-1<sup>+</sup> eTreg cells (pretreatment P = 0.76; after dCRT P = 0.63; after atezolizumab P = 0.90), CD80<sup>+</sup> HLA-DR<sup>+</sup> CD11c<sup>+</sup> cells (pretreatment P = 0.9995; after dCRT P = 0.9995; after atezolizumab P = 0.9995), CD86<sup>+</sup> HLA-DR<sup>+</sup> CD11c<sup>+</sup> cells (pretreatment P = 0.62; after dCRT P = 0.74; after atezolizumab P = 0.33), nor PD-L1<sup>+</sup> HLA-DR<sup>+</sup> CD11c<sup>+</sup> cells (pretreatment P = 0.46; after dCRT P = 0.08; after atezolizumab P = 0.46).



**Extended Data Fig. 7 | Immunological analysis of CBC during combination therapy with dCRT and atezolizumab.** Complete blood count (CBC) results from blood tests performed during treatment (pretreatment, post-dCRT, and post-atezolizumab treatment (cCR, N = 21 patients; non-cCR, N = 28 patients) were evaluated. Summaries of white blood cells (WBC) (upper left), neutrophils (upper middle), lymphocytes (upper right), and NLR (lower) during treatment (pretreatment, post-dCRT, and post-atezolizumab treatment) are shown according to treatment response. Red: patients who achieved cCR (cCR cases); black: patients who did not achieve cCR (non-cCR cases). Bars, mean; P values

were calculated using two-way analysis of variance. The Holm-Sidak test was performed for multiple comparisons. Between the cCR and non-cCR cases, significant differences after atezolizumab were found in neutrophils ( $P = 0.04$ ) and NLR ( $P = 0.006$ ), but there were no significant differences pretreatment (neutrophils  $P = 0.992$ ; NLR  $P = 0.95$ ) or after dCRT (neutrophils  $P = 0.58$ ; NLR  $P = 0.98$ ). Furthermore, there were no significant differences between the cCR and non-cCR cases at any time point in WBCs (pretreatment  $P = 0.93$ ; after dCRT  $P = 0.49$ ; after atezolizumab  $P = 0.13$ ) or lymphocytes (pretreatment  $P = 0.94$ ; after dCRT  $P = 0.57$ ; after atezolizumab  $P = 0.22$ ).



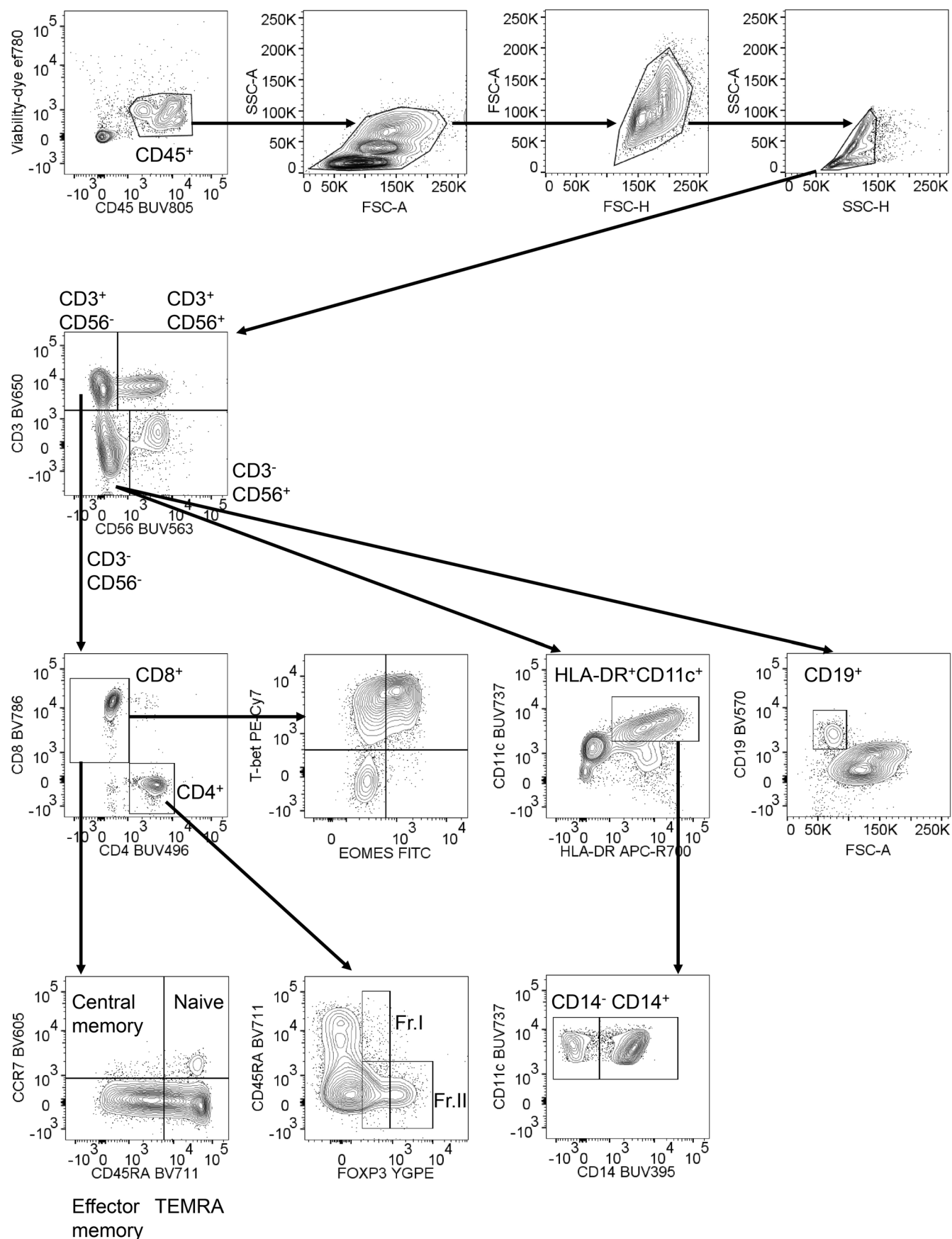
Extended Data Fig. 8 | See next page for caption.



**Extended Data Fig. 8 | Transcriptomic analysis of ESCCs according to treatment response after combination therapy with dCRT and atezolizumab.**

**(a)** Gene expression of *IL1A* (left) and *IL1B* (right) in ESCCs after combination therapy according to treatment response was examined by RNA-seq. Red, patients who achieved cCR (cCR cases) (N = 10); black, patients who did not achieve cCR (non-cCR cases) (N = 15). **(b)** Gene expression of ESCCs after combination therapy was evaluated according to treatment response by performing GSEA with the indicated gene sets. Plots showing the enrichment of IL-1R pathway-related genes (left upper), granulocyte pathway-related genes (left lower), the iCAF signature (right upper) and the CAF signature (right lower) are shown. **(c)** ssGSEA scores from the MDSC\_ShirleyLiu gene set were calculated from gene expression in ESCCs after combination therapy and compared according to treatment response was examined by RNA-seq. Red,

patients who achieved cCR (cCR cases) (N = 10); black, patients who did not achieve cCR (non-cCR cases) (N = 15). **(d)** Gene expression in ESCCs of non-cCR cases after combination therapy was compared with that in non-cCR ESCCs prior to treatment by performing GSEA. a plot showing the enrichment of CTLA-4 pathway-related genes is shown. **(e)** A graphic abstract of this translational study is shown. ESCCs with EMT phenotypes produce IL-1 $\beta$  in response to dCRT, leading to the induction of iCAFs and MDSCs and the activation of Treg cells (upper panel). As a result, these suppressive cells hamper the optimal antitumor immune response and cause resistance to sequential atezolizumab treatment. On the other hand, ESCCs without EMT phenotypes well respond to dCRT and sequential atezolizumab treatment. **(a and c)** P values were calculated by unpaired two-tailed t-test. Significant differences were found in *IL1A* (P = 0.003), *IL1B* (P = 0.03), and MDSC\_ShirleyLiu (P = 0.03) between the cCR and non-cCR cases.



**Extended Data Fig. 9 | Gating strategies for FCM analysis of patient samples.** Gating strategies for immune cells from PBMCs or TILs in FCM analysis are shown.

## Reporting Summary

Nature Portfolio wishes to improve the reproducibility of the work that we publish. This form provides structure for consistency and transparency in reporting. For further information on Nature Portfolio policies, see our [Editorial Policies](#) and the [Editorial Policy Checklist](#).

Please do not complete any field with "not applicable" or n/a. Refer to the help text for what text to use if an item is not relevant to your study. For [final submission](#): please carefully check your responses for accuracy; you will not be able to make changes later.

### Statistics

For all statistical analyses, confirm that the following items are present in the figure legend, table legend, main text, or Methods section.

n/a	Confirmed
<input type="checkbox"/>	<input checked="" type="checkbox"/> The exact sample size ( <i>n</i> ) for each experimental group/condition, given as a discrete number and unit of measurement
<input type="checkbox"/>	<input checked="" type="checkbox"/> A statement on whether measurements were taken from distinct samples or whether the same sample was measured repeatedly
<input type="checkbox"/>	<input checked="" type="checkbox"/> The statistical test(s) used AND whether they are one- or two-sided <i>Only common tests should be described solely by name; describe more complex techniques in the Methods section.</i>
<input type="checkbox"/>	<input checked="" type="checkbox"/> A description of all covariates tested
<input type="checkbox"/>	<input checked="" type="checkbox"/> A description of any assumptions or corrections, such as tests of normality and adjustment for multiple comparisons
<input type="checkbox"/>	<input checked="" type="checkbox"/> A full description of the statistical parameters including central tendency (e.g. means) or other basic estimates (e.g. regression coefficient) AND variation (e.g. standard deviation) or associated estimates of uncertainty (e.g. confidence intervals)
<input type="checkbox"/>	<input checked="" type="checkbox"/> For null hypothesis testing, the test statistic (e.g. <i>F</i> , <i>t</i> , <i>r</i> ) with confidence intervals, effect sizes, degrees of freedom and <i>P</i> value noted <i>Give P values as exact values whenever suitable.</i>
<input checked="" type="checkbox"/>	<input type="checkbox"/> For Bayesian analysis, information on the choice of priors and Markov chain Monte Carlo settings
<input checked="" type="checkbox"/>	<input type="checkbox"/> For hierarchical and complex designs, identification of the appropriate level for tests and full reporting of outcomes
<input checked="" type="checkbox"/>	<input type="checkbox"/> Estimates of effect sizes (e.g. Cohen's <i>d</i> , Pearson's <i>r</i> ), indicating how they were calculated

Our web collection on [statistics for biologists](#) contains articles on many of the points above.

### Software and code

Policy information about [availability of computer code](#)

Data collection	Microsoft Excel was used for data collection.
Data analysis	Data analyses were performed using SAS software version 9.4, R version 4.2.2, and GraphPad Prism v.9. All codes used in the analyses described in this study were based on existing tools and software, and no custom software, programs, or scripts were used. We have uploaded the code used in the analyses to Github, accessible at the following link: <a href="https://github.com/CancerImmunologyNCC/Bando_et_al_2024_RNAseq">https://github.com/CancerImmunologyNCC/Bando_et_al_2024_RNAseq</a> .

For manuscripts utilizing custom algorithms or software that are central to the research but not yet described in published literature, software must be made available to editors and reviewers. We strongly encourage code deposition in a community repository (e.g. GitHub). See the Nature Portfolio [guidelines for submitting code & software](#) for further information.

### Data

Policy information about [availability of data](#)

All manuscripts must include a [data availability statement](#). This statement should provide the following information, where applicable:

- Accession codes, unique identifiers, or web links for publicly available datasets
- A description of any restrictions on data availability
- For clinical datasets or third party data, please ensure that the statement adheres to our [policy](#)

All exome and transcriptome data have been deposited in the NBDC Human Database (<https://humandbs.dbcls.jp/en/hum0294-v1>). The accession numbers are JGAS000708 for the study and JGAD000841 for the dataset. These data are subject to restricted access and available only to researchers who have submitted a data usage application and have had their application approved. If one wishes to use this data, one must submit a data usage application through the application system. The procedure is described in the following website: <https://humandbs.dbcls.jp/en/data-use>. Use of the data is subject to the NBDC Human Data Sharing Guidelines and the NBDC Human Data Handling Security Guidelines (for data users). The hg38 dataset was accessed from the following link: [https://www.gencodegenes.org/human/release\\_34.html](https://www.gencodegenes.org/human/release_34.html). Source data for Fig. 2, 3, 4, and 5 and Extended Data for Fig. 2, 3, 4, 5, 6, 7, 8, and 9 are provided as Source Data files. All other data supporting the findings of this study are available from the corresponding author upon reasonable request.

# Research involving human participants, their data, or biological material

Policy information about studies with [human participants or human data](#). See also policy information about [sex, gender \(identity/presentation\), and sexual orientation](#) and [race, ethnicity and racism](#).

Reporting on sex and gender	Participants enrolled in this clinical trial includes 41 men and 9 women. No sex-based analyses have been performed because there have been no data regarding the difference of efficacies of IO and survival between male and female in ESCC. The sex / gender of participants was determined based on participants' self-reporting.
Reporting on race, ethnicity, or other socially relevant groupings	All of the participants enrolled in this clinical trial were Japanese.
Population characteristics	All patients had histologically confirmed unresectable locally advanced primary ESCC. In the primary cohort, median age was 64 years, and 82.5% (33/40) of the patients were male. A total of 95.0% (38/40) of patients had clinical T4 disease, and 92.5% (37/40) had lymph node metastasis. Furthermore, 25.0% (10/40) of the patients had extra-regional M1 lymph node metastasis.
Recruitment	Patients with unresectable locally advanced ESCC who were treated with 2 cycles of cisplatin/5-FU plus 60 Gy of radiation were enrolled. We sequentially registered cases that met the eligibility criteria from each clinical trial site, and we believe that there was no self-selection bias or other significant recruitment biases.
Ethics oversight	This study was approved by the ethics committees at each institution (National Cancer Center Institutional Review Board, Aichi Cancer Center Institutional Review Board, Saitama Cancer Center Review Board, Shizuoka Cancer Center Review Board, and the Cancer Institute Hospital of Japanese Foundation for Cancer Research Review Board). All patients were required to sign written informed consent forms.

Note that full information on the approval of the study protocol must also be provided in the manuscript.

## Field-specific reporting

Please select the one below that is the best fit for your research. If you are not sure, read the appropriate sections before making your selection.

☒ Life sciences ☐ Behavioural & social sciences ☐ Ecological, evolutionary & environmental sciences

For a reference copy of the document with all sections, see [nature.com/documents/nr-reporting-summary-flat.pdf](https://www.nature.com/documents/nr-reporting-summary-flat.pdf)

## Life sciences study design

All studies must disclose on these points even when the disclosure is negative.

Sample size	We calculated the sample size of the primary locally advanced ESCC cohort at 38 with a cCR of 40% deemed promising and one of 20% deemed unacceptable (one-sided $\alpha$ , 0.05; $\beta$ , 0.2).
Data exclusions	All the data acquired in this clinical trial were analyzed.
Replication	Since this was a single arm phase study, the specimens were collected from patients only once at each time point, and the amount of each specimen collected was very small. Thus, it was not possible to repeat the validation experiments.
Randomization	Randomization was not performed. The study focused on a limited group of patients with unresectable locally advanced esophageal squamous cell carcinoma, and it was challenging to secure a sufficient number of cases for randomization to evaluate the efficacy and safety of the trial treatment.
Blinding	Blinding was not performed. This was a non-randomised study without blinding of outcome assessments.

## Behavioural & social sciences study design

All studies must disclose on these points even when the disclosure is negative.

Study description	N/A
Research sample	N/A
Sampling strategy	N/A
Data collection	N/A
Timing	N/A
Data exclusions	N/A
Non-participation	N/A
Randomization	N/A



# Ecological, evolutionary & environmental sciences study design

All studies must disclose on these points even when the disclosure is negative.

Study description	N/A
Research sample	N/A
Sampling strategy	N/A
Data collection	N/A
Timing and spatial scale	N/A
Data exclusions	N/A
Reproducibility	N/A
Randomization	N/A
Blinding	N/A

Did the study involve field work? ☐ Yes ☒ No

## Field work, collection and transport

Field conditions	N/A
Location	N/A
Access & import/export	N/A
Disturbance	N/A

## Reporting for specific materials, systems and methods

We require information from authors about some types of materials, experimental systems and methods used in many studies. Here, indicate whether each material, system or method listed is relevant to your study. If you are not sure if a list item applies to your research, read the appropriate section before selecting a response.

Materials & experimental systems		Methods	
n/a	Involved in the study	n/a	Involved in the study
<input type="checkbox"/>	<input checked="" type="checkbox"/> Antibodies	<input checked="" type="checkbox"/>	<input type="checkbox"/> ChIP-seq
<input checked="" type="checkbox"/>	<input type="checkbox"/> Eukaryotic cell lines	<input type="checkbox"/>	<input checked="" type="checkbox"/> Flow cytometry
<input checked="" type="checkbox"/>	<input type="checkbox"/> Palaeontology and archaeology	<input checked="" type="checkbox"/>	<input type="checkbox"/> MRI-based neuroimaging
<input checked="" type="checkbox"/>	<input type="checkbox"/> Animals and other organisms		
<input type="checkbox"/>	<input checked="" type="checkbox"/> Clinical data		
<input type="checkbox"/>	<input checked="" type="checkbox"/> Dual use research of concern		
<input checked="" type="checkbox"/>	<input type="checkbox"/> Plants		

## Antibodies

Antibodies used	
Validation	We previously validated antibodies used in this study in our lab. The antibodies commercially available were validated by the manufacturers and used according to the manufacturer's instructions.

Cells (PBMCs and TILs) were washed using washing solution and subjected to staining with surface antibodies, including the anti-CTLA-4 antibody (1:50 dilution). The antibodies used in this study were described in the online methods section of the manuscript and supplementary table 7. Cells were stained with antibodies against CD3 (clone: SP7, ab16669, Abcam, Cambridge, UK, 1:200), CD8 (clone: C8/144B, M710301-2, Agilent, Santa Clara, CA, 1:200), FOXP3 (clone: 236A/E7, ab96048, Abcam, 1:100), Cytokeratin (clone: AE1 + AE3, ARG56129, Arigo Biolaboratories, Hsinchu, Taiwan, 1:200), and PD-1 (clone: EPR4877/2, ab137132, Abcam, 1:50). Anti-CD11c antibody was diluted to 1:50. For the FCM analyses, the following target molecules were involved: EOMES (clone: WD1928, eBioscience, 1:50); Ki67 (clone: B56, BD, 1:50); TCF1 (clone: 7F11A10, BioLegend, 1:50); HLA-DR (clone: L243, BioLegend, 1:50); PD1 (clone: MH4, BD, 1:50); CD80 (clone: 2D10, BioLegend, 1:50); CD19 (clone: HB19, BioLegend, 1:50); CCR7 (clone: G043H7, BioLegend, 1:50); CD3 (clone: UCHL1, BD, 1:50); CD45RA (clone: HI100, BioLegend, 1:50); CD8a (clone: RPA-T8, BioLegend, 1:50); CD14 (clone: M5E2, BD, 1:50); CD4 (clone: SK3, BD, 1:50); CD56 (clone: NCAM16.2, BD, 1:50); PD-L1 (clone: MH1, BD, 1:50); CD11c (clone: B4y6, BD, 1:50); CD45 (clone: HB3, BD, 1:50); FOXP3 (clone: 236A/E7, eBioscience, 1:50); CTLA-4 (clone: L3D10, BioLegend, 1:50); CD86 (clone: 2331 (FUN-1), BD, 1:50); Tbet (clone: eBio4B10, eBioscience, 1:50).

## Eukaryotic cell lines

Policy information about [cell lines and Sex and Gender in Research](#)

Cell line source(s)	N/A
Authentication	N/A
Mycoplasma contamination	N/A
Commonly misidentified lines (See <a href="#">ICLAC</a> register)	N/A

## Palaeontology and Archaeology

Specimen provenance	N/A
Specimen deposition	N/A
Dating methods	N/A
<input type="checkbox"/> Tick this box to confirm that the raw and calibrated dates are available in the paper or in Supplementary Information.	
Ethics oversight	N/A

Note that full information on the approval of the study protocol must also be provided in the manuscript.

## Animals and other research organisms

Policy information about [studies involving animals](#); [ARRIVE guidelines](#) recommended for reporting animal research, and [Sex and Gender in Research](#)

Laboratory animals	N/A
Wild animals	N/A
Reporting on sex	N/A
Field-collected samples	N/A
Ethics oversight	N/A

Note that full information on the approval of the study protocol must also be provided in the manuscript.

## Clinical data

Policy information about [clinical studies](#)

All manuscripts should comply with the ICMJE [guidelines for publication of clinical research](#) and a completed [CONSORT checklist](#) must be included with all submissions.

Clinical trial registration	We registered the study at the University Hospital Medical Information Network (clinical trial information number: UMIN000034373).
Study protocol	We briefly described the protocol of this study in the section of "Study design and treatments". In addition, the full study protocol has been provided.
Data collection	The data center of the Clinical Research Support Office, National Cancer Center Hospital East (NCCHE-OCRS), confirmed patient eligibility; data collection, analyses, and interpretation were also performed by the NCCHE-OCRS. Seven institutions including National Cancer Center Hospital East, National Cancer Center Hospital, Saitama Cancer Center, Cancer Institute Hospital of JFCR, Shizuoka Cancer Center, and Aichi Cancer Center participated in this study. The enrolment period was from December 2018 to March 2021, and the study was completed in January 2022.
Outcomes	Primary outcome: In patients with unresectable locally advanced esophageal squamous cell carcinoma, achieving a complete response (CR) after chemoradiotherapy has been clearly associated with long-term prognosis, and the CR rate is considered a surrogate endpoint for long-term prognosis. Secondary outcomes: We evaluated progression-free survival and overall response rate as alternative endpoints to CR, as well as overall survival as the true endpoint. Safety was also assessed.

## Dual use research of concern

Policy information about [dual use research of concern](#)

### Hazards

Could the accidental, deliberate or reckless misuse of agents or technologies generated in the work, or the application of information presented in the manuscript, pose a threat to:

- ☒ ☐ Public health  
☒ ☐ National security  
☒ ☐ Crops and/or livestock  
☒ ☐ Ecosystems  
☒ ☐ Any other significant area

## Experiments of concern

Does the work involve any of these experiments of concern:

- |                                     |  |
|-------------------------------------|--|
| No                                  | Yes  |
| <input checked="" type="checkbox"/> | <input type="checkbox"/> Demonstrate how to render a vaccine ineffective                             |
| <input checked="" type="checkbox"/> | <input type="checkbox"/> Confer resistance to therapeutically useful antibiotics or antiviral agents |
| <input checked="" type="checkbox"/> | <input type="checkbox"/> Enhance the virulence of a pathogen or render a nonpathogen virulent        |
| <input checked="" type="checkbox"/> | <input type="checkbox"/> Increase transmissibility of a pathogen                                     |
| <input checked="" type="checkbox"/> | <input type="checkbox"/> Alter the host range of a pathogen  |
| <input checked="" type="checkbox"/> | <input type="checkbox"/> Enable evasion of diagnostic/detection modalities                           |
| <input checked="" type="checkbox"/> | <input type="checkbox"/> Enable the weaponization of a biological agent or toxin                     |
| <input checked="" type="checkbox"/> | <input type="checkbox"/> Any other potentially harmful combination of experiments and agents         |

## Plants

Seed stocks	N/A
Novel plant genotypes	N/A
Authentication	N/A

## ChIP-seq

### Data deposition

- ☐ Confirm that both raw and final processed data have been deposited in a public database such as [GEO](#).  
☐ Confirm that you have deposited or provided access to graph files (e.g. BED files) for the called peaks.

Data access links <i>May remain private before publication.</i>	N/A
Files in database submission	N/A
Genome browser session (e.g. <a href="#">UCSC</a> )	N/A

### Methodology

Replicates	N/A
Sequencing depth	N/A
Antibodies	N/A
Peak calling parameters	N/A
Data quality	N/A
Software	N/A

## Plots

Confirm that:

- ☒ The axis labels state the marker and fluorochrome used (e.g. CD4-FITC).
- ☒ The axis scales are clearly visible. Include numbers along axes only for bottom left plot of group (a 'group' is an analysis of identical markers).
- ☒ All plots are contour plots with outliers or pseudocolor plots.
- ☒ A numerical value for number of cells or percentage (with statistics) is provided.

## Methodology

- Sample preparation Cells (PBMCs and TILs) were washed using washing solution and subjected to staining with surface antibodies (1:50 dilution). Intracellular staining of some molecules was performed with the corresponding antibodies and the Foxp3/Transcription Factor Staining Buffer Set.
- Instrument Cells were analyzed with a FACSymphony (BD Biosciences).
- Software FlowJo software (Treestar, Ashland, OR) was used.
- Cell population abundance All the cells obtained from PBMCs and TILs were analyzed.
- Gating strategy The gating strategy used in this study is shown in Extended Data Fig. 9
- ☒ Tick this box to confirm that a figure exemplifying the gating strategy is provided in the Supplementary Information.

## Magnetic resonance imaging

## Experimental design

- Design type N/A
- Design specifications N/A
- Behavioral performance measures N/A
- Imaging type(s) N/A
- Field strength N/A
- Sequence & imaging parameters N/A
- Area of acquisition N/A
- Diffusion MRI ☐ Used ☒ Not used

## Preprocessing

- Preprocessing software N/A
- Normalization N/A
- Normalization template N/A
- Noise and artifact removal N/A
- Volume censoring N/A

## Statistical modeling &amp; inference

- Model type and settings N/A
- Effect(s) tested N/A
- Specify type of analysis: ☐ Whole brain ☐ ROI-based ☐ Both



Statistical type for inference

N/A

(See [Eklund et al. 2016](#))

Correction

N/A

## Models & analysis

n/a | Involved in the study

- ☒ ☐ Functional and/or effective connectivity
- ☒ ☐ Graph analysis
- ☒ ☐ Multivariate modeling or predictive analysis

Functional and/or effective connectivity

N/A

Graph analysis

N/A

Multivariate modeling and predictive analysis

N/A

